Soft Electronics for the Skins: from Health Monitors to Human-Machine Interfaces

*Zhoulyu Rao, Faheem Ershad, Abdullah Almasri, Lei Gonzalez, Xiaoyang Wu, Cunjiang Yu**

Z. Rao, Prof. C. Yu
Materials Science and Engineering Program
University of Houston
Houston, TX, 77204 USA

F. Ershad, A. Almasri, L. Gonzalez, Prof. C. Yu
Department of Biomedical Engineering
University of Houston
Houston, TX, 77204 USA

Prof. X. Wu
Ben May Department for Cancer Research
The University of Chicago
Chicago, IL, 60637 USA

Prof. C. Yu
Department of Mechanical Engineering
Department of Electrical and Computer Engineering
Texas Center for Superconductivity
University of Houston
Houston, TX, 77204 USA
E-mail: cyu15@uh.edu

Keywords: Soft electronics, stretchable electronics, skin, health monitoring, human-machine interfaces

Abstract

Conventional bulky and rigid electronics prevents compliant interfacing with soft human skin for health monitoring and human-machine interaction, due to the incompatible mechanical characteristics. To overcome the limitations, soft skin-mountable electronics with superior mechanical softness, flexibility, and stretchability provides an effective platform for intimate interaction with humans. In addition, soft electronics offers comfortability when worn on the soft, curvilinear, and dynamic human skin. In this review, recent advances in soft electronics as health monitors and human-machine interfaces (HMIs) are briefly discussed. Strategies to achieve softness in soft electronics including structural designs, material innovations, and approaches to optimize the interface between human skin and soft electronics are briefly reviewed. Characteristics and performances of soft electronic devices for health monitoring, including temperature sensors, pressure sensors for pulse monitoring, pulse oximeters, electrophysiological sensors, and sweat sensors, exemplify their wide range of utility. Furthermore, we review the soft devices for prosthetic limb, household object, mobile machine, and virtual object control to highlight the current and potential implementations of soft electronics for a broad range of HMI applications. This review concludes with a discussion on the current limitations and future opportunities of soft skin-mountable electronics.

1. Introduction

Electronics for human health monitoring and human-machine interaction has evolved over time, transforming from large and bulky equipment to miniature and portable devices for daily usage. Devices such as the traditional Holter monitor, the gold standard for cardiac electrophysiology at one point, have been packaged into wearable and portable formats that could be attached to the human body with a strap.[1, 2] Many other devices, including wearable accelerometers for motion detection, electromyography (EMG) sensors for prosthetics, electroencephalography (EEG) sensors for brain-machine interfaces, and smart gloves for robot/machine control have been developed.[3-6] However, the aforementioned electronics exists in rigid form factors and must be uncomfortably secured to the human body.[2, 7, 8] The mechanical mismatch that arises from the rigid electronics hinders the movement of the body, creates user discomfort, and increases the susceptibility to motion artifacts.[9]

To better suit the skin, soft electronics offers an alternative route for conformal interfacing and comfortable wearing on the soft, curvilinear, and dynamic human body. Soft skin-mountable electronics have been proven to be effective for various applications including medical implants, health monitors, artificial skins, human-machine interfaces (HMIs), wearable internet-of-things (IoT), etc. due to their superior mechanical properties. Here, soft electronics comprises the characteristics of both flexibility and stretchability.

Various approaches to realizing soft skin-mountable electronics have been implemented and since these strategies have been extensively reviewed in the literature, they will be briefly mentioned here. It is understood that to achieve flexibility, the electronics should be sufficiently thin in order to undergo deformations such as bending or folding.[10] Adequate thickness and minimization of the conformal energy can result in conformal contact between the skin and the electronics. On the other hand, realizing stretchability is a more complicated feat. Generally, two strategies are utilized to impart stretchability; these include designing electronics with

geometrically engineered structures or the use of intrinsically stretchable materials. A few examples of structural engineering strategies used to achieve in-plane/out-of-plane stretchability are wrinkles, serpentines,[11] rigid islands with deformable interconnects, and kirigami structures.[12-14] Achieving stretchability with intrinsically stretchable materials has also been appealing, and thus, efforts to develop intrinsically stretchable conductors, semiconductors, and dielectrics have been undertaken.[15-17]

In this review, we begin with a brief overview of the approaches to optimize the interface between human skin and soft electronics. In particular, we highlight the applicability of soft skin-mountable electronics for health monitoring and human-machine interaction. In each of these sections, numerous studies are detailed with an emphasis on the device characteristics and performance for their respective applications. For health monitoring, studies showing vitals measured using soft temperature sensors, pressure sensors for pulse monitoring, pulse oximeters, electrophysiological sensors, and sweat sensors are presented. Following that section, soft HMI devices used for prosthetic limb, household object, mobile machine, and virtual object control are discussed. We conclude with a discussion on the current limitations and future opportunities of soft skin-mountable electronics.

2. Strategies to Improve the Soft Electronics/Skin Interface

Biological skin is soft, flexible, twistable, and stretchable with a low modulus of 140-160 kPa and an elastic tensile strength of 15-30%.[10, 18] Robust and conformal contact with the surface of skin is required for soft electronics which should have similar mechanical properties to the skin. In other words, soft skin-mountable electronics should be flexible and stretchable to comply with deformation of the skin and accommodate local strains during daily activities. However, traditional electronics made with bulky and brittle materials is not compatible for this purpose. Thus, soft, flexible, and stretchable electronics has been recently developed to

interface with skin for applications such as regenerative medicine, health monitoring,[19, 20] and HMIs.[21] These types of electronics hold advantages like high-quality data collection, minimal irritation to the human skin, and compatible integration with IoT technologies.[22]

Certain approaches have been implemented to realize soft electronics as compliant, multifunctional skins for humans and robots. To achieve mechanical softness, one effective approach is to reduce the bending stiffness of electronics by making them thin: the bending stiffness of a structure is proportional to its thickness raised to the third power.[23] For example, brittle yet thin silicon (fracture limit of 1%)[24, 25] with 100-nm thickness is mechanically flexible and can be bent while remaining intact.[26] In addition to imparting flexibility to electronic devices, they also require mechanical stretchability to better interface and concurrently deform with the skin. Two strategies have been applied to achieve mechanical stretchability in soft electronics: 1) utilizing intrinsically stretchable materials including rubbery electronic materials (semiconductors, conductors, and dielectrics),[15, 17, 27-38] liquid metals[39-42] to build the electronics; 2) employing engineered structures like wrinkles,[26, 43-49] serpentines,[10, 25, 37, 50-55] island–bridge structures,[56, 57] textiles,[58] origami,[59, 60] kirigami,[29, 61] microcracks,[62] etc., to accommodate the induced strain.[22, 63-66]

In addition to enabling softness in soft electronics, it is critical to ensure the electronics/skin conformity and adhesion when electronics is mounted onto skin. The surface of human skin is microscopically rough with wrinkles, creases, and pits. Through the attachment of soft skin-mountable electronics structured in ultrathin films, open-meshes, and microstructures to the skin, increased conformity to the epidermal topography has been achieved.[67-69] For example, a membrane with 5-μm thickness can conformably contact a skin model, while air gaps were formed when the thicker membranes were applied (**Figure 1**a).[70] Someya et al. successfully reduced the total thickness of their devices down to sub-300 nm, as shown in Figure 1b.[67, 71] Due to their ultrathin thickness, the devices were self-adhesive to the

skin and had comparable bending stiffness to the stratum corneum, making them capable of monitoring of EMG signals with reduced motion artifacts. Additionally, epidermal electronics with an open-mesh layout, which provides low effective elastic moduli, can also achieve similar results (Figure 1c).[72]

Microstructure designs were also introduced to increase conformity and adhesion to the topography of human skin. Inspired by a gecko-mimicking structure, Bao et al. applied microhair structures to develop a highly flexible pressure sensor (Figure 1d).[73] The long hairs tended to bend and interlock to match the profile of the skin when the external pressure was applied. The microhair structures effectively reduced the voids between the sensors and pig skin; microhairs with an aspect ratio of 10 can almost fully cover (98% coverage) the macroscopically rough surface of the pig skin. By means of this intimate contact, the pressure sensor was able to detect deep jugular venous pulses (JVP) from a human subject. Other bio-inspired adhesive structures have also been utilized as adhesive layers to enhance the adhesion of the devices to skin[74, 75]. For example, Ha et al. developed a flexible temperature sensor based on an octopus suction cup inspired adhesive polydimethylsiloxane (PDMS) substrate which is non-irritating, long-lasting, and recyclable (Figure 1e).[74] Another approach to impart adhesion lies in engineering the device substrate is by tuning it to achieve the desired physical and chemical properties. For example, by adding a curing inhibitor and conductive carbon-nanotubes (CNTs), the PDMS became stickier, conductive, and softer, enabling a high-quality recording of ECG signal, as shown in Figure 1f.[75, 76]

3. Soft Health Monitoring Sensors

With healthcare spending and utilization increasing, especially over the past decades, it has become increasingly imperative that health monitoring devices meet the demands of the global population.[77] The uptick in devices connected to the IoT has driven the development of

portable, wearable devices.[78, 79] Today, most of the commercially available wearable health monitoring devices, such as smart watches, exist in rigid formats. The device-skin interface can have air cavities and is not necessarily electrically stable.[80] Soft skin-mountable electronics substantially improves the device-skin interface and possesses the advantages of deformability, imperceptibility, and comfortability as compared to its rigid counterpart.[22] Here, we discuss soft sensors including temperature sensors, pressure sensors for pulse monitoring, electrophysiological sensors, pulse oximeters, and sweat sensors that are used to monitor several key parameters of the human body.

3.1. Temperature Sensors

Temperature of the skin indicates the state of the human body and reveals useful diagnostic information. Abnormal body temperatures are correlated to human diseases like inflammation and fever.[81-83] To comply with the human skin, temperature sensors should be non-toxic, unnoticeable, and mechanically soft to ensure minimal harm to the skin and high-quality signal detection.[22]

The existing temperature sensors are mainly based on various thermistors,[10, 84, 85] and thermosensitive field effect transistors (FETs).[86, 87] The simplest and most widely used thermistors are metallic and metal oxide filamentary wires,[88] due to their excellent antioxidation property and good linearity below 300°C.[89] Rogers et al. used ultrathin and filamentary serpentine gold (**Figure 2**a) as a temperature sensor on skin to derive the core body temperature with a precision of ~20 mK.[84] A similar electronic sensing platform was exploited to monitor temperature and thermal conductivity of skin at multiple sites near a wound, as shown in Figure 2b.[83] The results revealed that temperature of skin adjacent to the cutaneous wound site suddenly rose on the third day after surgery due to increased blood flow and enzymatic reactions, which are correlated to the inflammation phase. At the same time, the

thermal conductivity of skin near the wound decreased slightly compared to the normal skin, indicating a variation of the hydration state around the hypersensitive wound tissue. In addition, active monitoring of both the thermal conductivity and thermal diffusivity of the skin was demonstrated by mapping the local thermal distribution induced by micro-thermal heaters laminated on the skin.[90] Temperature sensors can also be exploited as thermal flow sensors to obtain the arterial blood flow rate .[91] Aside from metals, other materials, in various physical formats, including but not limited to graphene,[75, 92] CNTs,[93] conducting polymers,[94] and self-healing hydrogels[95] have also been used for temperature sensing and further designed to improve sensitivity. Thermosensitive materials for temperature measurement can also be integrated into FETs to achieve signal amplification and higher signal-to-noise ratio (SNR). Ha et al. exploited a poly (N-isopropylacrylamide) (PNIPAM) hydrogel to develop a thermosensitive FET, in which the gate was coated on the PNIPAM suspended on top of the channel, as shown in Figure 2c.[86] The PNIPAM hydrogel deswelled to bend towards to the channel with increasing temperature, and the air gap between the gate and active channel decreased, resulting in an increase in the drain current under a constant voltage. By means of this strategy, a high sensitivity of 0.065/°C could be achieved.

In order to improve the interface between the temperature sensors and skin while simultaneously allowing for real-time, comfortable, and continuous temperature measurement during daily movements, soft temperature sensors have been developed.[96, 97] Therefore, architecturally engineered designs like strain-island structures,[86] in-plane serpentines,[98] and kirigami structures[85] have been employed to decouple the strain effect and minimize the cross-sensitivity during temperature measurement. Ha et al. placed temperature sensitive FETs on PET islands arranged on a stretchable PDMS substrate to make the temperature sensor 50% biaxially stretchable without performance degradation (Figure 2d).[86] Besides, Lee et al. also fabricated thermosensitive reduced graphene oxide/polyurethane (PU) composite fibers into

serpentine structures to construct a strain-insensitive stretchable temperature sensor.[98] The device on a stretchable bandage (Figure 2e,f) showed stable *in vivo* temperature monitoring of skin with a high resolution of 0.1°C during various body motions. Additionally, Liu et al. 3D-printed thermosensitive graphene/PDMS ink into kirigami architectures including grid, triangular, and hexagonal porous structures to accommodate the external strain during movement (Figure 2g).[85] The composites with a grid structure showed a sensitivity of 0.008/ºC. Another approach to improve the accuracy of the temperature measurement is to suppress the strain using differential voltage read-out circuit designs without structural engineering (Figure 2h).[99] As a result, this differential sensing circuit under a static condition can achieve a sensitivity of -24.2 mV/°C and a sensing resolution of 0.5°C for body temperature sensing. This stretchable temperature sensor showed less than +1°C variation under uniaxial strain up to 60%.

3.2. Pressure Sensors

Soft pressure sensors detect external blood pressure changes on the skin which are correlated to vital cardiovascular information such as heart sounds, blood pressure (BP), pulse rate, and respiration rate.[73, 100, 101] In addition, these sensors should be light-weight, provide detailed diagnostics, and mobile long-term monitoring for early-stage diagnosis of cardiovascular diseases like hypertension.[102] For example, a flexible pressure-sensitive organic FET was utilized to monitor the pulse wave of an adult human radial artery in real time and three distinguishable peaks could be observed in the pulse wave: the systolic peak, diastolic peaks, and diastolic tail, which indicate the ejection of blood by the left ventricle, ventricular relaxation, and constriction of the aorta, respectively (**Figure 3**a).[103] Important cardiovascular information including heart beating rate, arterial stiffness (the time delay between systolic and diastolic peaks), and radial augmentation index (ratio of systolic and diastolic peaks) were

determined.[103-106] Another example is the detection of the deep internal JVP (Figure 3b) which is valuable for diagnosis of cardiac failure or hypervolemia.[73]

Pressure detection is mainly based on piezoresistive,[107] piezocapacitive,[108, 109] and piezoelectric[110] effects. The simplest forms of piezoresistive pressure sensors are composites of conductive fillers and insulating elastomers. Lee et al. reported a pressure sensitive composite of sea urchin-shaped metal nanoparticles and PU elastomer with excellent mechanic flexibility and robust durability (Figure 3c).[111] Due to the spike shape of the metallic nanoparticles, the quantum tunneling effect was enhanced,[112] and the sensor achieved a sensitivity of 2.46 kPa^{-1} (Figure 3d). To further improve the performance of pressure sensor, microstructures were introduced. Chung et al. introduced a micro pyramids structured PDMS array to develop a flexible pressure sensor with an ultrahigh sensitivity of 10.3 kPa^{-1}, a low detection limit of 23 Pa under 40% stretch, and capability of non-invasive detection of the pulse (Figure 3e,f).[104] The sensitivity of this sensor was improved by the enlarged contact area of two electrodes induced by deformation of PDMS pyramids when they were pressed. When the pressure was relieved, pyramids recovered to their initial states due to their elastomeric nature. Additionally, a conical frustum-like PDMS microstructures based pressure sensor was created by Yang et al. to detect the pulse waves. The P-wave (percussion), T-wave (tidal) and D-wave (diastolic) peaks of the human pulse waveform could all be observed, as shown in Figure 3g,h.[113] Other types of surface microstructures like microdomes,[114] microhumps,[115] and micro-semicylinders[116] were also exploited on elastomers.

For piezocapacitive pressure sensors, the pressure change is indicated by the capacitance change without current flow and therefore, little power is consumed.[117] The piezocapacitive pressure sensors were built with two electrodes separated by elastomeric dielectrics.[118] The pressure sensors can also be integrated into FETs to achieve signal amplification.[106, 119] Zhu et al. presented an organic ultra-sensitive flexible pressure sensing FET with a suspended gate

(Figure 3i).[106] After inducing pressure on the gate, the capacitance increased, leading to an increased current between the source and drain. Thus, the pressure variations were amplified by the FET, which showed a high sensitivity (192 kPa^{-1}), a low limit-of-detection (0.5 Pa), and fast response (10 ms), as shown in Figure 3j. This device showed the capability of detecting acoustic waves in real time. Additionally, two-dimensional semiconducting materials were utilized to improve the amplified pressure sensitivity.[119]

Piezoelectric materials offer another alternative for pressure sensing due to their high sensitivity, excellent SNR, and self-powered ability.[120] Lee et al. developed a highly sensitive flexible and stretchable piezoelectric pressure sensor which achieved sufficient compliance and mechanically deformed with the skin (Figure 3k). The sensor successfully detected pulse waves from the radial and carotid arteries in real time, with clearly defined features such as the P, T and D waves.[121]

3.3. Pulse Oximeters

Pulse oximetry, a non-invasive and continuous method to assess the pulse rate and the oxygen saturation in arterial blood (SaO_2), is based on the different light absorptions of oxyhemoglobin (HbO_2) and deoxyhemoglobin (Hb) at two different wavelengths. In practice, two lights with different wavelengths are alternatively shined into the skin with a frequency of 1 kHz, and then the lights are either transmitted (transmission mode) or reflected (reflection mode) to a photodetector. Red (640 nm) and near infrared (914 nm) light are normally used, but other combinations of lights like green and red were also proven to successfully obtain pulse rate.[122-124] The SaO_2 is given by

$$SaO_2 = \frac{k_1 - k_2 R}{k_3 - k_4 R},$$

where R is the ratio of the ratios of the diastolic (AC) and systolic (DC) peaks in the two different light absorption spectra, $R = \frac{(AC/DC)_1}{(AC/DC)_2}$, and k_i are the constants related to the molar absorptions of Hb and HbO_2, which are determined in the calibration process.[125]

Conventional clinical pulse oximeters are bulky and rigid. To overcome limitations of the commercial pulse oximeters, Arias et al. created a flexible transmission oximeter with green (532 nm) and red (626 nm) organic light emitting diodes (OLEDs) and organic photodiodes (PDs), which were integrated on a flexible plastic substrate wrapped around a finger (**Figure 4**a).[122] The OLEDs and PDs were distributed on opposite sides of a finger and the PDs effectively detected transmitted lights and delivered a clear photoplethysmogram (PPG) signal, showing accurate heart beating rate (1% error) and SaO_2 (2% error) compared to a commercial transmission pulse oximeter.

The application of transmission pulse oximeters is limited to only peripheral tissues, such as the earlobes and fingertips, which the light can penetrate through. Furthermore, the PPG signal in these peripheral tissues is most easily weakened, especially in medical emergencies.[126] In contrast, reflection pulse oximeters can be mounted on a diverse range of body parts, such as the forearm, chest, and forehead due to the LEDs and PDs arrangement on the same side.[124, 127] Reflection oximeters are resistive to unfavorable health conditions like massive ischemia, low blood perfusion, and low peripheral temperature and can reliably monitor SaO_2.[126] Arias et al. developed a flexible 4 × 4 organic oximeter array consisting of green (532 nm) and red (626 nm) LEDs and PDs printed on a 125-µm polyethylene naphthalate (PEN) substrate (Figure 4b).[128] During normal conditions, the single oximeter worked in reflection mode, showing the strongest pulsatile signal on the forehead with a mean error of 1.1% of SaO_2, compared to the finger probe transmission pulse oximeter. In addition, by inducing a temporary ischemic condition on the forearm with an absent pulsatile PPG signal, the reflectance mode oximeter array (which employed a modified calculation model)

successfully measured the change in oxygen saturation, while standard pulse oximetry in neither transmission nor reflection modes could measure the change. Another ultrathin reflection pulse oximeter with total thickness of 3 μm was also developed to improve the adhesion to skin, resulting in little noise and good repeatability of the PPG signal measurement.[123] Reflection mode pulse oximeters offer a promising approach to achieve imperceptible integration on skin with few motion artifacts.

Moreover, reflection mode pulse oximeters combined with micro-sized wireless data and power transmission systems hold potential for chronic monitoring in the hospital and at-home diagnostics. Rogers et al. innovated a soft, stretchable, battery-free, and fully wireless optoelectronic system including a reflection pulse oximeter capable of monitoring heart rate, tissue oxygenation, and pressure pulse dynamics, shown in Figure 4c.[127, 129] The power and data were delivered and transmitted via magnetic inductive coupling and near-field communication (NFC) schemes, enabling the transmission of data to portable devices like a smartphone and a wearable electronic watch.

3.4. Electrophysiological Sensors

Soft electrophysiological sensors (EP) which are used to measure the biopotentials or currents elicited by the activities of different organs, such as the heart (ECG), brain (EEG), and muscles (EMG), hold great promise in applications like early detection, diagnosis, and recovery monitoring of the corresponding diseases.[19, 102, 130] The morphology of the ECG waveform is a strong indicator of a compromised heart. Abnormal shapes observed from the subwaves of the ECG (P, QRS, and T waves) reveal arrhythmias such as P wave asystole (no ventricular activity), lengthened QRS waves (abnormal heart rate), and T wave abnormalities (could indicate myocardial ischemia).[131, 132] Studies of EEG signals or signals from deeper anatomical structures in the brain elucidate the origins of epilepsy or Parkinson's, diseases which

significantly deter the quality of life for the aging population.[133, 134] EP sensors for EMG measurement are typically used to monitor neuromuscular activity and can identify nerve and muscle dysfunction.[135] Various forms of soft EP sensors have been developed to monitor both healthy and diseased individuals.

The conventional EP sensors typically come in the form of wet gel Ag/AgCl electrodes which have shown good signal quality.[136-138] However, they tend to dry out, causing degradation in signal, and are limited for long-term usage.[138] Alternative options are dry conductive materials including metals,[139] carbon materials,[140] conductive polymers,[141] and their hybrids. These materials can be used to easily achieve comfortable wearing, long-term monitoring, and minimal skin irritation.[67, 142] However, developing devices with high signal quality remains challenging. To overcome this, methods to reduce skin-electrode impedance and motion artifacts induced by electrode movement have been implemented. Vörös et al. fabricated stretchable polymeric Ag microparticle/Ecoflex composite electrodes for ECG and EEG evaluation (**Figure 5**a).[142] The electrodes, which were based on soft silicone materials with a modulus similar to that of skin, can enlarge the effective contact area. As a result, they can compensate for the microscopic roughness, and effectively reduce the skin-electrode impedance. Moreover, in order to mitigate motion artifacts and improve the comfortability, a micro-pillar structure was introduced into the conductive materials to improve the adhesion up to 0.1 N/cm due to Van der Waals interactions between the tips of the pillars and the skin surface. This cuff-free, self-adhesive electrode showed a high SNR ECG signal with clearly distinguishable P, QRS, and T peaks while the subject was swimming. Microstructures such as octopus-like suckers were also adopted to improve the adhesion.[143] However, these microstructures normally involve porous surface designs which sacrifice the effective electrode area and thereby increase skin-electrode impedance. Someya et al. exploited another method in which 300 nm thin film electrodes were laminated on the skin (Figure 5b).[67] They reported

that the thinner film on the artificial skin had a higher roughness akin to the skin, which resulted in a larger contact area with the skin. This ultraconformal contact successfully reduced the impedance to 55 kΩ at steady state and increased the peel strength (135.09 mN/cm) required to remove the electrodes from the skin. The ultrathin electrodes were used to demonstrate motion artifact-less recording and monitoring of EMG signals over 10 hours.

3.5. Sweat Sensors

Biomarkers in sweat have a quantitative correlation to their in-body counterparts: for example, 0.3 mM glucose in sweat corresponds to 300 mg dL^{-1} glucose in blood.[144] Thus, sweat diagnostics has been used to assess the states of in-body biomarkers to study the dynamics of body metabolism and physiology.[145, 146] Soft sweat sensors enable sweat analysis as an effective and non-invasive approach for biomedical applications including drug monitoring and diagnosis of diseases.[147-150] Although sweat sensors with different operation mechanisms have been developed, sensors that operate based on electrochemical methods have been extensively exploited.[148, 151-153] The biomarkers experience electrochemical reactions at the electrodes and the induced electrical parameter changes quantitatively indicate the concentration of the biomarkers.[148, 154, 155] These sensors have the advantages of high sensitivity and selectivity, low response times, minimal irritation, and ease of fabrication. Recently, various soft electrochemical sensors have been demonstrated for analysis of a wealth of sweat biomarkers including electrolyte ions, metabolic molecules, and small proteins and peptides.[156-158]

The research interest is mainly focused on the improvement of sensitivity, selectivity, adaptation to skin, and comfortability.[159, 160] For example, Kim et al. reported a stretchable diabetes monitoring patch consisting of an electrochemical glucose sensor and pH sensor (**Figure 6**a).[147] They innovated Ag doped graphene to improve the electrochemical sensitivity. The glucose oxidase enzyme immobilized on Au doped graphene electrodes was used for

selective glucose determination and a serpentine interconnection was adapted to realize the stretchable patch. However, the enzymes used for selective detection of the corresponding biomarkers are normally costly, unstable, and difficult to immobilize. Thus, non-enzyme sensors have been proposed as an alternative. Various nanomaterials, like metals, metal alloys, and transition metal oxides have recently been verified to react with biomarkers with high sensitivity.[161] A non-enzyme, stretchable $CoWO_4$ based glucose sensor and polyaniline (PANI) based pH sensors were developed by Ha et al.[162] The authors used all intrinsically stretchable materials and the device showed a stretchability of 30% with a glucose sensitivity of 10.89 μA/mM·cm^2 and a pH sensitivity of 71.44 mV/pH (Figure 6b). Selectivity could be achieved by controlling the potential below 0.3 V, which only allowed for oxidation of the glucose.[162]

Considering factors such as small amounts, low secretion, rapid evaporation, and contamination from skin,[157] obtaining fresh sweat is important for sensitivity and reliability of the measurement. Microfluidic devices mounted on skin have been utilized to collect and temporarily store sweat.[156, 163] Wang et al. created an epidermal electrochemical sensing and a soft microfluidic platform for real-time continuous monitoring of sweat metabolites like lactate and glucose during cycling. In addition, after electrochemical detection, the researchers realized real-time data transmission of the concentration of the metabolites using a Bluetooth controller (Figure 6c).[164] Furthermore, Rogers et al. developed a well-designed microfluidic and reservoir system that could harvest sweat and route it to different channels for sensing the biomarkers of interest. Data was transferred using a wireless interface to external devices for image capture and analysis to determine the concentration of the biomarkers.[163]

4. Soft HMI Devices

HMIs facilitate bidirectional communication between humans and computers, robots, or other machines through sensing and feedback.[9, 21] As discussed in the previous section, various modes of data acquisition from the body are possible and each modality provides unique information about the health of the skin, internal organs, and/or the overall human body. An HMI can utilize these signals to provide various types of feedback to the user such as electrical, optical, audio, physical, or visual stimulation.[9] Traditionally, HMI devices took rigid formats, but due to their poor comfortability, restrictions to body movement, and inability to adapt to the deformation created from bodily motions, HMI devices based on soft electronics are superior alternatives. Below, we review the various types of existing soft HMI devices, which are not only implemented for human usage, but also for robot usage. These devices consist of soft tactile sensors, motion sensors, and/or EP sensors that enable human-machine interaction. The following studies are organized into specific applications of HMIs: prosthetic limb, household object, mobile machine, and virtual object control.

4.1. Prosthetic Limb Control

Prosthetic limbs are central to assisting those with reduced limb function or limb amputations. The typical strategy for rehabilitation of limbs involves locating the active nerve fibers (recording EMG) near the site of injury and applying electrical stimulation them.[135] Locating the injury sites requires the use of EP sensors, as discussed in a previous section. For the affected patients, electrical stimulation simulates the sensations that would be perceived from the missing limb.[165, 166] However, it is often the case that the muscle requiring innervation and monitored skin sites are in the same locations and conventional, bulky electrodes fail to be effective in these circumstances.[80, 167] Aside from EMG based prosthetics, tactile and motion sensors have also found use in prosthetic limb control.[168, 169] These soft electronics based HMI devices have offered new avenues for interfacing with human users for control of prosthetics,

enhancing the development in robotics, virtual reality, and healthcare as evidenced by the following studies. In this section, we specifically describe soft tactile, motion, and EP sensors used for prosthetic control without and with feedback.

Tactile, motion, and EP sensors have been utilized for prosthetic limb control. Typically, these sensors are utilized only for prosthetic limbs that are limited to certain functions, such as gripping, and have a limited range of motion.[168] An approach that resulted in more nuanced control of robotic arm movement was reported by Lee et al. By placing their self-powered, flexible, triboelectric sensor (SFTS) on the forearm and finger of a human subject (**Figure 7**a), the authors could control the velocity, acceleration, and trajectory of a robotic arm and thus, realize a 3D detection and control system. The starch-based hydrogel/silicon rubber-based devices (Figure 7b) allowed the subject to draw different letters on a whiteboard by controlling the robotic arm (Figure 7c,d). Tactile sensors have also been utilized for controlling soft prosthetics.[170] For example, Hong et al. developed a soft robotic hand that was controlled by a printed assembly of surface-mounted devices connected by epoxies and stretchable Ag interconnects, all on PDMS (Figure 7e,f). This combination of stretchable hybrid electronics exploited the current progress in the development of miniaturized integrated circuits and electronic components for real-time communication between the soft HMI device developed for the human subject (control skin) and the soft robotic hand (Figure 7g, h). The control skin had embedded pressure sensors that responded to pressing and correspondingly caused the fingers of the robotic hand to bend. EP sensors have also been utilized to control wearable prosthetics. It should be noted that a limitation to this approach of prosthetic control is the area of sensing, which is usually a few square centimeters. Thus, efforts to increase the size of the devices have been undertaken.[80] Rogers et al. created large-area (40-fold larger than electronics shown in previous studies) epidermal electronics based on fractal mesh electrodes encapsulated by polyimide (PI). The devices were supported by two layers of silicone rubber

for adhesion and were released onto skin (Figure 7i). This is an alternate approach for lamination onto the skin, unlike the previously discussed works which utilized polyvinyl alcohol as a holder substrate that was removed using water. The large-area electronics were placed on an amputated upper limb for movement classification using EMG signals (Figure 7j). Various movements generated different patterns of EMG activity (Figure 7k). The classification accuracy of the signals attained from the large-area electrodes was shown to be greater than that of the conventional, rigid electrodes, which indicated that the reported devices have better signal acquisition capabilities than the conventional devices. So far, all the aforementioned studies have been limited to prosthetic limb control without feedback to the user.

To achieve closed-loop control, it is necessary to provide stimulation to the human user to facilitate teaming between humans and machines. Various approaches combine temperature, motion, tactile, and/or electrophysiological sensors with stimulators that offer feedback to the user. Our group recently developed a multifunctional HMI device to demonstrate signal transmission between a human user and a robotic system (**Figure 8**a).[54] The multifunctional HMI device is based on indium zinc oxide (IZO) as the active material to enable functions including data storage, switching, and temperature, ultraviolet, and strain sensing. The imperceptible HMI devices were worn on the user's forearm (Figures 8b) and a robotic hand (Figure 8c). When the robotic hand touched an object and detected its temperature (Figure 8d,e), a proportional amount of stimulation was applied to a heater (Figure 8f) worn by the human user. In this manner, the user could directly perceive the detected temperature from the robotic hand, as an example of virtual reality. Furthermore, the robotic hand could be controlled with motion sensors that detected the strain induced by movements of the user's hand (Figure 8g). Motion sensors have also been combined with electrical stimulation to provide feedback to the user. Kim et al. constructed a closed-loop, interactive HMI based on transparent and stretchable piezoelectric motion sensors and electrotactile stimulators schematically shown in Figure

8h.[169] The motion sensor was based on a layer of SWNTs embedded into polylactic acid (PLA), all encapsulated by graphene and poly(methyl methacrylate) (PMMA). The main components of the stimulator were the graphene/AgNW/graphene layer sandwiched by epoxy, all on PDMS as the substrate. The heterostructure of the stimulator provided enhanced conductivity and charge injection.[171] After programming a robotic manipulator to respond to certain commands, the researchers demonstrated relaxing, bending, and pressing of the piezoelectric motion sensor on the human arm as methods to control the configuration of the robot (Figure 8i,j). When the detected voltage from the motion sensor crossed a certain threshold, the robot could grip the object. As the robot was equipped with a pressure sensor, it caused the stimulator to apply electrical stimulation to the human user when the object was sufficiently gripped, in order to prevent excessive gripping. EP sensors have also been implemented with electrical stimulators to control robotic grippers. Rogers and co-workers fabricated simple EMG sensors and electrical stimulation devices by patterning serpentine Cr/Au onto a silicone rubber.[172] Usually, stimulation artifacts plague electrical potential recordings, so digital filters were applied to reduce observed artifacts. To highlight the versatility of the soft HMI device, feedback stimulation for controlling a grip force of a robotic hand, prevention of muscle overexertion through EMG monitoring and stimulation feedback, and induced muscle contractions for revitalizing limbs were all realized (Figure 8k-m).

4.2. Household Object Control

To improve convenience of living, smart home systems that operate based on noncontact and tactile sensors have been developed.[173] These sensors typically require interaction with the human body but are not used to monitor the underlying biological activity beneath the human skin. Soft noncontact and tactile sensors which are highly sensitive, have fine spatial resolution, and show fast response times enable the development of HMI devices that can be suitable for

daily use. The soft HMI devices must also conformably adhere to the wearer and operate normally under the associated deformations.[174] Furthermore, HMI devices based on TENGs have been developed for both noncontact and tactile interaction.[175-177]

Breath-based HMIs have been developed by Mao et al. to realize household object control which is schematically illustrated in **Figure 9**a.[176] The TENG was activated by the breathing of the user and the signals were processed and transmitted to the appliance (Figure 9b). The signal produced by the TENG, the switched square signal, and the electrical power are plotted in the top, middle, and bottom of the graph in Figure 9c, respectively. As a demonstration, a subject controlled the power of a light fixture (Figure 9d,e) and a fan. Other types of sensors can be used for noncontact interaction.[177] Additionally, TENGs have also been implemented for tactile usage. A washable electronic textile (WET) comprised of two layers of fabric (silk and nylon) that sandwiched a printed layer of PU/CNT electrodes has been fabricated.[178] After immersing the WET in water for 15 hours, the authors concluded that there was negligible change in the square resistance of the CNT electrodes. In addition to controlling a program developed in LabView with finger gestures on the WET, the authors demonstrated their device as a trigger to control home appliances such as light bulbs, fans, and microwaves (Figure 9f). Other HMIs based on TENGs, such as those developed by Wang and co-workers, enable control of household objects via bodily motions such as eye movement.[173] The soft mechanosensing TENGs (msTENGs) were based on fluorinated ethylene propylene as one of the electrification layers and natural latex as the other electrification layer, which directly contacted the skin. Indium tin oxide (ITO) and PET served as the back electrode and substrate, respectively (Figure 9g). The mechanism of operation of the msTENG is shown in Figure 9h. Household objects such as a table lamp, electric fan, and doorbell were controlled by eye movements (Figure 9i).

4.3. Mobile Machine Control

Controlling mobile machines through HMIs enables remote operation and improved quality of life. In addition to TENGs, soft pressure sensor based HMIs have been fabricated for robot navigation.[179-181] Furthermore, sensing of the electrical potentials generated by eye movement, or electrooculagraphy, has been an important approach for controlling mobile machines. By implementing machine learning to classify the EP signals obtained from the soft sensors, subjects have been able to maneuver drones and wheelchairs.[70, 182, 183]

Pressure sensors and EP sensors have successfully been implemented to control the direction of movement of various mobile machines. Kim et al. mixed a reverse micelles solution into pressure sensitive rubber to introduce pores, otherwise referred to as porous pressure sensitive rubbers (PPSRs), and increased their deformability, thereby increasing their sensitivity.[180] Pressure sensors and strain gauges based on films of PPSR sandwiched by conductive carbon fabrics were adhered onto a finger and forearm of a human subject. The user could control the acceleration/deceleration of a mobile robot by bending fingers and causing deformations captured by the strain gauges (**Figure 10**a). Forward/backward movement and clockwise/counterclockwise rotation were controlled with four pressure sensors. Other methods of motion control based on TENGs and EP sensors have been investigated.[181] Electrooculography (EOG) is particularly useful for brain and sleep studies, assistive technology, and developing HMIs. EOG, despite its less complex nature compared to EEG and EMG, still involves the use of bulky, stiff, and uncomfortable sensing equipment that patients must wear. Lu and co-workers reported an ultrathin, transparent, and biocompatible EOG graphene electronic tattoo (GET) shown schematically in Figure 10b.[183] Four GETs were laminated around the eye without additional adhesives and provided high-precision EOG sensing with an angular resolution of 4° (Figure 10c). Different types of eye movements coded for various commands (Figure 10d). By interfacing the GETs with an OpenBCI biosensing

board, a human subject was able to use eye movements to control the flight of a quadcopter in three dimensions, as shown in Figure 10e. In addition, eye movements were used to demonstrate the hands-free control of a robotic wheelchair (Figure 10f).[182] The classification algorithm demonstrated comparable accuracy (Figure 10g,h) of the soft, fractal structured devices and the conventional rigid electrodes.

4.4. Virtual Object Control

Alongside motion control of machines in real environments, control of virtual objects has been realized through soft, wearable HMIs. Again, tactile, motion, and EP sensors have been worn by human users to enable virtual control. These soft HMIs can be used for a variety of applications including military, industrial, agricultural, medical, marine, rescue, and smart home robots, although a few applications are discussed. The soft virtual object control HMIs enable improved quality of life for both healthy and diseased individuals.[184-188]

Tactile and motion sensors have proven to be useful for virtual object control. One of the current limitations of conventional touch panels is that they utilize stiff and brittle electrodes.[184]An ionic touch panel made from polyacrylamide (PAAm) hydrogel and lithium chloride (LiCl) salts was developed by Sun et al. (**Figure 11**a).[184] The principle of operation shown in Figure 11b illustrates the current flow from the ionic touch panel to the finger, due to the finger being grounded. The device operated at 100% strain without losing functionality and was demonstrated for writing words and playing touchpad games, presented in Figure 11c. Malliaras and co-workers also developed a textile based HMI.[185] Their wearable keyboard was fabricated by patterning conductive poly(3,4-ethylenedioxythiophene): poly(styrene sulfonate), or PEDOT:PSS, onto a knitted textile and then coating the brush-painted electrodes with PDMS (Figure 11d). The stretchable capacitive sensors functioned under 20% strain and showed little performance degradation. The wearable keyboard could easily distinguish between the pressed

sensors even when worn on the forearm of a human subject, indicating a high spatial resolution (Figure 11e). In addition to tactile sensing, motion sensing has allowed for virtual control. Lee et al. constructed a glove-based HMI using PEDOT:PSS coated textiles, as shown in Figure 11f.[186] By bending the PEDOT:PSS TENG, different voltage responses could be obtained (Figure 11g). Through the different motions of the glove, the subjects were able to draw letters in a computer program (Figure 11h) and scroll through a website (Figure 11i,j).

EP sensors have been deployed for brain-computer interfacing and object manipulation in videogames. Rogers et al. demonstrated long-term epidermal (LTE) electrodes based on Au and PI that were designed in fractal layouts and placed on multiple locations on the head of subject for EEG recording (**Figure 12**a).[187] The use of liquid bandage spray to coat the LTE electrodes created a more durable and robust interface that was suited for usage over 2 weeks, with regular application of the spray. After mounting the electrodes onto skin, the authors ran a speller-based paradigm on the subjects to train an algorithm that could predict the letters of a word from the acquired EEG signals (Figure 12b). In this case, the subjects tried to spell the word 'computer' and the algorithm showed similar classification results for both the LTE and conventional electrodes (Figure 12c). Another paradigm was developed based on the principle of steady-state visually evoked potentials, which arise in specific areas of the brain in response to visual stimuli.[189] By flashing different characters across the screen and observing the EEG signals obtained with the LTE electrodes, the algorithm could classify the desired letter based on the subject's focus and thoughts (Figure 12d). Mechano-acoustic sensing is another manner by which virtual control has been established.[188] Another stretchable hybrid electronic device, developed by Rogers and co-workers, was used for detection of speech signals from the vocal cord (Figure 12e). The classified signals were then used to control a virtual character in a videogame (Figure 12f).

5. Conclusion

We have summarized here only a small fraction of the recent advances in soft skin-mountable electronics utilized for health monitoring and human-machine interfacing. Soft electronics offers a refined approach to modernizing the technologies that directly interface with the human body and can be comparable in terms of performance to the conventional, bulky, and rigid electronics. In addition to overcoming the inconsistent and unreliable interface of rigid electronics, soft electronics also maintains low profiles, intimate contact, and a robust interface with the dynamic human body. The superior mechanical properties of soft skin-mountable electronics have enabled usage in numerous applications such as health monitors,[163] human-machine interfaces,[13, 21, 54, 80, 127, 188, 190-192] medical implants,[102, 123, 193-199] wearable IoT,[200-203] and artificial skins.[17, 31, 33, 127, 194, 195, 204-207]

Though soft skin-mountable electronics are promising alternatives to the existing technologies, as discussed in this review, to realize soft health monitors and HMIs with both high performance and uniformity is still challenging. As discussed earlier, stretchable electronics developed through structural engineering still faces the drawbacks of complex design and fabrication and large-area consumption due to the stretchable interconnection. The drawbacks make high-density integration, packaging, and low-cost mass production more difficult to achieve. Although intrinsically stretchable materials could be preferable alternatives, the intrinsically stretchable devices and electronics have shown relatively lower performances as compared to some of the structurally engineered devices. Some of the developed soft skin-mountable electronics and their associated devices have great potential, but they have not fully matured, nor have they achieved widespread usage due to the aforementioned limitations.

Future efforts in the development of soft skin-mountable electronics will tackle these challenges. Through thorough investigation, comprehensive knowledge and understanding of the material structure-property relationships and requirements for manufacturing high

performance materials and devices can be acquired and determined. Alongside the materials considerations, dependable and scalable device manufacturing and packaging technologies are required for soft electronics to be realized for their broad applications and real-world usage. The ongoing efforts to develop and advance soft electronics from various aspects predicate improved human health monitoring and human-machine interaction devices in the near future.

Acknowledgements

Z.R. and F.E. contributed equally to this work. C.Y. would like to thank the National Science Foundation CAREER grant (CMMI-1554499), the Doctoral New Investigator grant from American Chemical Society Petroleum Research Fund (56840-DNI7), the Office of Naval Research grant (N00014-18-1-2338) under Young Investigator Program and 3M non-tenured faculty award. F.E. would like to acknowledge the National Science Foundation Graduate Research Fellowship Program.

Received: ((will be filled in by the editorial staff))
Revised: ((will be filled in by the editorial staff))
Published online: ((will be filled in by the editorial staff))

References

[1] S. S. Lobodzinski, *Prog. Cardiovasc. Dis.* **2013**, *56*, 224.
[2] R. Fensli, E. Gunnarson, T. Gundersen, presented at 18th IEEE Symposium on Computer-Based Medical Systems (CBMS'05), June **2005**.
[3] F. Lotte, L. Bougrain, A. Cichocki, M. Clerc, M. Congedo, A. Rakotomamonjy, F. Yger, *J. Neural Eng.* **2018**, *15*, 031005.
[4] E. M. Tapia, S. S. Intille, W. Haskell, K. Larson, J. Wright, A. King, R. Friedman, presented at 2007 11th IEEE International Symposium on Wearable Computers, Oct. **2007**.
[5] E. A. Brackbill, Y. Mao, S. K. Agrawal, M. Annapragada, V. N. Dubey, presented at 2009 IEEE International Conference on Robotics and Automation, May **2009**.
[6] I. Choi, E. W. Hawkes, D. L. Christensen, C. J. Ploch, S. Follmer, presented at 2016 IEEE/RSJ International Conference on Intelligent Robots and Systems (IROS), Oct. **2016**.
[7] F. Benito-Lopez, S. Coyle, R. Byrne, A. Smeaton, N. E. O'Connor, D. Diamond, *Procedia Chem.* **2009**, *1*, 1103.

[8] N. Watthanawisuth, T. Lomas, A. Wisitsoraat, A. Tuantranont, presented at ECTI-CON2010: The 2010 ECTI International Confernce on Electrical Engineering/Electronics, Computer, Telecommunications and Information Technology, May **2010**.
[9] W. Dong, Y. Wang, Y. Zhou, Y. Bai, Z. Ju, J. Guo, G. Gu, K. Bai, G. Ouyang, S. Chen, Q. Zhang, Y. Huang, *Int. J. Intell. Robot. Appl.* **2018**, *2*, 313.
[10] D.-H. Kim, N. Lu, R. Ma, Y.-S. Kim, R.-H. Kim, S. Wang, J. Wu, S. M. Won, H. Tao, A. Islam, K. J. Yu, T.-i. Kim, R. Chowdhury, M. Ying, L. Xu, M. Li, H.-J. Chung, H. Keum, M. McCormick, P. Liu, Y.-W. Zhang, F. G. Omenetto, Y. Huang, T. Coleman, J. A. Rogers, *Science* **2011**, *333*, 838.
[11] C. Wang, K. Sim, J. Chen, H. Kim, Z. Rao, Y. Li, W. Chen, J. Song, R. Verduzco, C. Yu, *Adv. Mater.* **2018**, *30*, 1706695.
[12] S. Xu, Z. Yan, K.-I. Jang, W. Huang, H. Fu, J. Kim, Z. Wei, M. Flavin, J. McCracken, R. Wang, A. Badea, Y. Liu, D. Xiao, G. Zhou, J. Lee, H. U. Chung, H. Cheng, W. Ren, A. Banks, X. Li, U. Paik, R. G. Nuzzo, Y. Huang, Y. Zhang, J. A. Rogers, *Science* **2015**, *347*, 154.
[13] J. Kim, M. Lee, H. J. Shim, R. Ghaffari, H. R. Cho, D. Son, Y. H. Jung, M. Soh, C. Choi, S. Jung, K. Chu, D. Jeon, S.-T. Lee, J. H. Kim, S. H. Choi, T. Hyeon, D.-H. Kim, *Nat. Commun.* **2014**, *5*, 5747.
[14] M. Isobe, K. Okumura, *Sci. Rep.* **2016**, *6*, 24758.
[15] Y. Wang, C. Zhu, R. Pfattner, H. Yan, L. Jin, S. Chen, F. Molina-Lopez, F. Lissel, J. Liu, N. I. Rabiah, Z. Chen, J. W. Chung, C. Linder, M. F. Toney, B. Murmann, Z. Bao, *Sci. Adv.* **2017**, *3*, e1602076.
[16] A. T. Kleinschmidt, D. J. Lipomi, *Acc. Chem. Res.* **2018**, *51*, 3134.
[17] H. Shim, K. Sim, F. Ershad, P. Yang, A. Thukral, Z. Rao, H.-J. Kim, Y. Liu, X. Wang, G. Gu, L. Gao, X. Wang, Y. Chai, C. Yu, *Sci. Adv.* **2019**, *5*, eaax4961.
[18] V. Arumugam, M. D. Naresh, R. Sanjeevi, *J. Biosci.* **1994**, *19*, 307.
[19] Y. H. Lee, O. Y. Kweon, H. Kim, J. H. Yoo, S. G. Han, J. H. Oh, *J. Mater. Chem. C* **2018**, *6*, 8569.
[20] Z. Ma, S. Li, H. Wang, W. Cheng, Y. Li, L. Pan, Y. Shi, *J. Mater. Chem. B* **2019**, *7*, 173.
[21] J. Wang, M.-F. Lin, S. Park, P. S. Lee, *Mater. Today* **2018**, *21*, 508.
[22] C. Wang, C. Wang, Z. Huang, S. Xu, *Adv. Mater.* **2018**, *30*, 1801368.
[23] Y. Wyser, C. Pelletier, J. Lange, *Packag. Technol. Sci.* **2001**, *14*, 97.
[24] Y. Zhang, Z. Yan, K. Nan, D. Xiao, Y. Liu, H. Luan, H. Fu, X. Wang, Q. Yang, J. Wang, W. Ren, H. Si, F. Liu, L. Yang, H. Li, J. Wang, X. Guo, H. Luo, L. Wang, Y. Huang, J. A. Rogers, *Proc. Natl. Acad. Sci. USA* **2015**, *112*, 11757.
[25] K. Sim, S. Chen, Z. Li, Z. Rao, J. Liu, Y. Lu, S. Jang, F. Ershad, J. Chen, J. Xiao, C. Yu, *Nat. Electron.* **2019**, *2*, 471.
[26] W. M. Choi, J. Song, D.-Y. Khang, H. Jiang, Y. Y. Huang, J. A. Rogers, *Nano Lett.* **2007**, *7*, 1655.
[27] C. Hou, Z. Xu, W. Qiu, R. Wu, Y. Wang, Q. Xu, X. Y. Liu, W. Guo, *Small* **2019**, *15*, 1805084.
[28] P. Li, Y. Zhao, J. Ma, Y. Yang, H. Xu, Y. Liu, *Adv. Mater. Technol.* **2020**, *5*, 1900823.
[29] S.-H. Sunwoo, S. I. Han, H. Kang, Y. S. Cho, D. Jung, C. Lim, C. Lim, M.-j. Cha, S.-P. Lee, T. Hyeon, D.-H. Kim, *Adv. Mater. Technol.* **2020**, *5*, 1900768.
[30] K. Sim, Z. Rao, H.-J. Kim, A. Thukral, H. Shim, C. Yu, *Sci. Adv.* **2019**, *5*, eaav5749.
[31] H.-J. Kim, A. Thukral, S. Sharma, C. Yu, *Adv. Mater. Technol.* **2018**, *3*, 1800043.
[32] H.-J. Kim, A. Thukral, C. Yu, *ACS Appl. Mater. Interfaces* **2018**, *10*, 5000.
[33] H.-J. Kim, K. Sim, A. Thukral, C. Yu, *Sci. Adv.* **2017**, *3*, e1701114.

[34] N. Matsuhisa, D. Inoue, P. Zalar, H. Jin, Y. Matsuba, A. Itoh, T. Yokota, D. Hashizume, T. Someya, *Nat. Mater.* **2017**, *16*, 834.
[35] Y. Kim, J. Zhu, B. Yeom, M. Di Prima, X. Su, J.-G. Kim, S. J. Yoo, C. Uher, N. A. Kotov, *Nature* **2013**, *500*, 59.
[36] K. H. Lee, M. S. Kang, S. Zhang, Y. Gu, T. P. Lodge, C. D. Frisbie, *Adv. Mater.* **2012**, *24*, 4457.
[37] S. Wang, J. Xu, W. Wang, G.-J. N. Wang, R. Rastak, F. Molina-Lopez, J. W. Chung, S. Niu, V. R. Feig, J. Lopez, T. Lei, S.-K. Kwon, Y. Kim, A. M. Foudeh, A. Ehrlich, A. Gasperini, Y. Yun, B. Murmann, J. B. H. Tok, Z. Bao, *Nature* **2018**, *555*, 83.
[38] C. Yu, Y. Zhang, D. Cheng, X. Li, Y. Huang, J. A. Rogers, *Small* **2014**, *10*, 1266.
[39] Y. Lin, C. Cooper, M. Wang, J. J. Adams, J. Genzer, M. D. Dickey, *Small* **2015**, *11*, 6397.
[40] L. Zhu, B. Wang, S. Handschuh-Wang, X. Zhou, *Small* **2020**, *16*, 1903841.
[41] S. Zhu, J.-H. So, R. Mays, S. Desai, W. R. Barnes, B. Pourdeyhimi, M. D. Dickey, *Adv. Funct. Mater.* **2013**, *23*, 2308.
[42] M. D. Bartlett, A. Fassler, N. Kazem, E. J. Markvicka, P. Mandal, C. Majidi, *Adv. Mater.* **2016**, *28*, 3726.
[43] S. Chen, S. Peng, W. Sun, G. Gu, Q. Zhang, X. Guo, *Adv. Mater. Technol.* **2019**, *4*, 1800681.
[44] C. Yu, C. Masarapu, J. Rong, B. Wei, H. Jiang, *Adv. Mater.* **2009**, *21*, 4793.
[45] C. Yu, Z. Wang, H. Yu, H. Jiang, *Appl. Phys. Lett.* **2009**, *95*, 141912.
[46] C. Yu, K. O'Brien, Y.-H. Zhang, H. Yu, H. Jiang, *Appl. Phys. Lett.* **2010**, *96*, 041111.
[47] D.-Y. Khang, H. Jiang, Y. Huang, J. A. Rogers, *Science* **2006**, *311*, 208.
[48] H. Jiang, D.-Y. Khang, J. Song, Y. Sun, Y. Huang, J. A. Rogers, *Proc. Natl. Acad. Sci. USA* **2007**, *104*, 15607.
[49] Y. Sun, V. Kumar, I. Adesida, J. A. Rogers, *Adv. Mater.* **2006**, *18*, 2857.
[50] R. Feiner, L. Wertheim, D. Gazit, O. Kalish, G. Mishal, A. Shapira, T. Dvir, *Small* **2019**, *15*, 1805526.
[51] J. Kim, A. Banks, H. Cheng, Z. Xie, S. Xu, K.-I. Jang, J. W. Lee, Z. Liu, P. Gutruf, X. Huang, P. Wei, F. Liu, K. Li, M. Dalal, R. Ghaffari, X. Feng, Y. Huang, S. Gupta, U. Paik, J. A. Rogers, *Small* **2015**, *11*, 906.
[52] S. B. Kim, K. Lee, M. S. Raj, B. Lee, J. T. Reeder, J. Koo, A. Hourlier-Fargette, A. J. Bandodkar, S. M. Won, Y. Sekine, J. Choi, Y. Zhang, J. Yoon, B. H. Kim, Y. Yun, S. Lee, J. Shin, J. Kim, R. Ghaffari, J. A. Rogers, *Small* **2018**, *14*, 1802876.
[53] K. N. Noh, S. I. Park, R. Qazi, Z. Zou, A. D. Mickle, J. G. Grajales-Reyes, K.-I. Jang, R. W. Gereau Iv, J. Xiao, J. A. Rogers, J.-W. Jeong, *Small* **2018**, *14*, 1702479.
[54] K. Sim, Z. Rao, Z. Zou, F. Ershad, J. Lei, A. Thukral, J. Chen, Q.-A. Huang, J. Xiao, C. Yu, *Sci. Adv.* **2019**, *5*, eaav9653.
[55] K. Sim, Y. Li, J. Song, C. Yu, *Adv. Mater. Technol.* **2019**, *4*, 1800489.
[56] L. Yin, J. K. Seo, J. Kurniawan, R. Kumar, J. Lv, L. Xie, X. Liu, S. Xu, Y. S. Meng, J. Wang, *Small* **2018**, *14*, 1800938.
[57] H. C. Ko, M. P. Stoykovich, J. Song, V. Malyarchuk, W. M. Choi, C.-J. Yu, J. B. Geddes Iii, J. Xiao, S. Wang, Y. Huang, J. A. Rogers, *Nature* **2008**, *454*, 748.
[58] C. Luo, B. Tian, Q. Liu, Y. Feng, W. Wu, *Adv. Mater. Technol.* **2020**, *5*, 1900925.
[59] J. Rogers, Y. Huang, O. G. Schmidt, D. H. Gracias, *MRS Bull.* **2016**, *41*, 123.
[60] Z. Yan, F. Zhang, J. Wang, F. Liu, X. Guo, K. Nan, Q. Lin, M. Gao, D. Xiao, Y. Shi, Y. Qiu, H. Luan, J. H. Kim, Y. Wang, H. Luo, M. Han, Y. Huang, Y. Zhang, J. A. Rogers, *Adv. Funct. Mater.* **2016**, *26*, 2629.
[61] R. Sun, S. C. Carreira, Y. Chen, C. Xiang, L. Xu, B. Zhang, M. Chen, I. Farrow, F. Scarpa, J. Rossiter, *Adv. Mater. Technol.* **2019**, *4*, 1900100.

[62] Y. Guo, Z. Guo, M. Zhong, P. Wan, W. Zhang, L. Zhang, *Small* **2018**, *14*, 1803018.
[63] K. Sim, Z. Rao, F. Ershad, C. Yu, *Adv. Mater.* **2019**, *n/a*, 1902417.
[64] P. Li, H. P. Anwar Ali, W. Cheng, J. Yang, B. C. K. Tee, *Adv. Mater. Technol.* **2020**, *5*, 1900856.
[65] L. Li, Z. Lou, D. Chen, K. Jiang, W. Han, G. Shen, *Small* **2018**, *14*, 1702829.
[66] X. Wang, Z. Liu, T. Zhang, *Small* **2017**, *13*, 1602790.
[67] R. A. Nawrocki, H. Jin, S. Lee, T. Yokota, M. Sekino, T. Someya, *Adv. Funct. Mater.* **2018**, *28*, 1803279.
[68] K. Sim, S. Chen, Y. Li, M. Kammoun, Y. Peng, M. Xu, Y. Gao, J. Song, Y. Zhang, H. Ardebili, C. Yu, *Sci. Rep.* **2015**, *5*, 16133.
[69] A. Thukral, F. Ershad, N. Enan, Z. Rao, C. Yu, *IEEE Nanotechnology Magazine* **2018**, *12*, 21.
[70] J.-W. Jeong, W.-H. Yeo, A. Akhtar, J. J. S. Norton, Y.-J. Kwack, S. Li, S.-Y. Jung, Y. Su, W. Lee, J. Xia, H. Cheng, Y. Huang, W.-S. Choi, T. Bretl, J. A. Rogers, *Adv. Mater.* **2013**, *25*, 6839.
[71] R. A. Nawrocki, N. Matsuhisa, T. Yokota, T. Someya, *Adv. Electron. Mater.* **2016**, *2*, 1500452.
[72] W. H. Yeo, Y. S. Kim, J. Lee, A. Ameen, L. Shi, M. Li, S. Wang, R. Ma, S. H. Jin, Z. Kang, *Adv. Mater.* **2013**, *25*, 2773.
[73] C. Pang, J. H. Koo, A. Nguyen, J. M. Caves, M. G. Kim, A. Chortos, K. Kim, P. J. Wang, J. B. H. Tok, Z. Bao, *Adv. Mater.* **2015**, *27*, 634.
[74] J. H. Oh, S. Y. Hong, H. Park, S. W. Jin, Y. R. Jeong, S. Y. Oh, J. Yun, H. Lee, J. W. Kim, J. S. Ha, *ACS Appl. Mater. Interfaces* **2018**, *10*, 7263.
[75] Y. Yamamoto, D. Yamamoto, M. Takada, H. Naito, T. Arie, S. Akita, K. Takei, *Adv. Healthcare Mater.* **2017**, *6*, 1700495.
[76] S. H. Jeong, S. Zhang, K. Hjort, J. Hilborn, Z. Wu, *Adv. Mater.* **2016**, *28*, 5830.
[77] A. B. Martin, M. Hartman, B. Washington, A. Catlin, *Health Aff.* **2017**, *36*, 166.
[78] S. Feng, R. Caire, B. Cortazar, M. Turan, A. Wong, A. Ozcan, *ACS Nano* **2014**, *8*, 3069.
[79] D. J. Wile, R. Ranawaya, Z. H. T. Kiss, *J. Neurosci. Methods* **2014**, *230*, 1.
[80] L. Tian, B. Zimmerman, A. Akhtar, K. J. Yu, M. Moore, J. Wu, R. J. Larsen, J. W. Lee, J. Li, Y. Liu, B. Metzger, S. Qu, X. Guo, K. E. Mathewson, J. A. Fan, J. Cornman, M. Fatina, Z. Xie, Y. Ma, J. Zhang, Y. Zhang, F. Dolcos, M. Fabiani, G. Gratton, T. Bretl, L. J. Hargrove, P. V. Braun, Y. Huang, J. A. Rogers, *Nat. Biomed. Eng.* **2019**, *3*, 194.
[81] T. Q. Trung, H. S. Le, T. M. L. Dang, S. Ju, S. Y. Park, N.-E. Lee, *Adv. Healthcare Mater.* **2018**, *7*, 1800074.
[82] W. Gao, S. Emaminejad, H. Y. Y. Nyein, S. Challa, K. Chen, A. Peck, H. M. Fahad, H. Ota, H. Shiraki, D. Kiriya, D.-H. Lien, G. A. Brooks, R. W. Davis, A. Javey, *Nature* **2016**, *529*, 509.
[83] Y. Hattori, L. Falgout, W. Lee, S.-Y. Jung, E. Poon, J. W. Lee, I. Na, A. Geisler, D. Sadhwani, Y. Zhang, Y. Su, X. Wang, Z. Liu, J. Xia, H. Cheng, R. C. Webb, A. P. Bonifas, P. Won, J.-W. Jeong, K.-I. Jang, Y. M. Song, B. Nardone, M. Nodzenski, J. A. Fan, Y. Huang, D. P. West, A. S. Paller, M. Alam, W.-H. Yeo, J. A. Rogers, *Adv. Healthcare Mater.* **2014**, *3*, 1597.
[84] Y. Zhang, R. C. Webb, H. Luo, Y. Xue, J. Kurniawan, N. H. Cho, S. Krishnan, Y. Li, Y. Huang, J. A. Rogers, *Adv. Healthcare Mater.* **2016**, *5*, 119.
[85] Z. Y. Wang, W. L. Gao, Q. Zhang, K. Q. Zheng, J. W. Xu, W. Xu, E. W. Shang, J. Jiang, J. Zhang, Y. Liu, *ACS Appl. Mater. Interfaces* **2019**, *11*, 1344.
[86] S. Y. Hong, M. S. Kim, H. Park, S. W. Jin, Y. R. Jeong, J. W. Kim, Y. H. Lee, L. Sun, G. Zi, J. S. Ha, *Adv. Funct. Mater.* **2019**, *29*, 1807679.

[87] T. Q. Trung, S. Ramasundaram, S. W. Hong, N. E. Lee, *Adv. Funct. Mater.* **2014**, *24*, 3438.
[88] T. Q. Trung, N.-E. Lee, *Adv. Mater.* **2016**, *28*, 4338.
[89] C.-Y. Lee, C.-H. Lin, Y.-M. Lo, *Sensors* **2011**, *11*, 3706.
[90] R. C. Webb, R. M. Pielak, P. Bastien, J. Ayers, J. Niittynen, J. Kurniawan, M. Manco, A. Lin, N. H. Cho, V. Malyrchuk, *PLoS One.* **2015**, *10*, e0118131.
[91] R. C. Webb, Y. Ma, S. Krishnan, Y. Li, S. Yoon, X. Guo, X. Feng, Y. Shi, M. Seidel, N. H. Cho, J. Kurniawan, J. Ahad, N. Sheth, J. Kim, J. G. Taylor Vi, T. Darlington, K. Chang, W. Huang, J. Ayers, A. Gruebele, R. M. Pielak, M. J. Slepian, Y. Huang, A. M. Gorbach, J. A. Rogers, *Sci. Adv.* **2015**, *1*, e1500701.
[92] J. Yang, D. Wei, L. Tang, X. Song, W. Luo, J. Chu, T. Gao, H. Shi, C. Du, *RSC Adv.* **2015**, *5*, 25609.
[93] J. Di, X. Zhang, Z. Yong, Y. Zhang, D. Li, R. Li, Q. Li, *Adv. Mater.* **2016**, *28*, 10529.
[94] K. Kanao, S. Harada, Y. Yamamoto, W. Honda, T. Arie, S. Akita, K. Takei, *RSC Adv.* **2015**, *5*, 30170.
[95] J. Wu, S. J. Han, T. Z. Yang, Z. Li, Z. X. Wu, X. C. Gui, K. Tao, J. M. Miao, L. K. Norford, C. Liu, F. W. Huo, *ACS Appl. Mater. Interfaces* **2018**, *10*, 19097.
[96] T. Yokota, Y. Inoue, Y. Terakawa, J. Reeder, M. Kaltenbrunner, T. Ware, K. Yang, K. Mabuchi, T. Murakawa, M. Sekino, *Proc. Natl. Acad. Sci. USA* **2015**, *112*, 14533.
[97] T. Q. Trung, S. Ramasundaram, B.-U. Hwang, N.-E. Lee, *Adv. Mater.* **2016**, *28*, 502.
[98] T. Q. Trung, T. M. L. Dang, S. Ramasundaram, P. T. Toi, S. Y. Park, N. E. Lee, *ACS Appl. Mater. Interfaces* **2019**, *11*, 2317.
[99] C. X. Zhu, A. Chortos, Y. Wang, R. Pfattner, T. Lei, A. C. Hinckley, I. Pochorovski, X. Z. Yan, J. W. F. To, J. Y. Oh, J. B. H. Tok, Z. A. Bao, B. Murmann, *Nat. Electron.* **2018**, *1*, 183.
[100] S. J. Chen, B. G. Zhuo, X. J. Guo, *ACS Appl. Mater. Interfaces* **2016**, *8*, 20364.
[101] K. Meng, J. Chen, X. Li, Y. Wu, W. Fan, Z. Zhou, Q. He, X. Wang, X. Fan, Y. Zhang, J. Yang, Z. L. Wang, *Adv. Funct. Mater.* **2019**, *29*, 1806388.
[102] Y. Liu, M. Pharr, G. A. Salvatore, *ACS Nano* **2017**, *11*, 9614.
[103] G. Schwartz, B. C. K. Tee, J. Mei, A. L. Appleton, D. H. Kim, H. Wang, Z. Bao, *Nat. Commun.* **2013**, *4*, 1859.
[104] C. L. Choong, M. B. Shim, B. S. Lee, S. Jeon, D. S. Ko, T. H. Kang, J. Bae, S. H. Lee, K. E. Byun, J. Im, *Adv. Mater.* **2014**, *26*, 3451.
[105] W. W. Nichols, *Am. J. Hypertens.* **2005**, *18*, 3S.
[106] Y. Zang, F. Zhang, D. Huang, X. Gao, C.-a. Di, D. Zhu, *Nat. Commun.* **2015**, *6*, 6269.
[107] J. Shi, L. Wang, Z. Dai, L. Zhao, M. Du, H. Li, Y. Fang, *Small* **2018**, *14*, 1800819.
[108] Y. Xiong, Y. Shen, L. Tian, Y. Hu, P. Zhu, R. Sun, C.-P. Wong, *Nano Energy* **2020**, *70*, 104436.
[109] W. Asghar, F. Li, Y. Zhou, Y. Wu, Z. Yu, S. Li, D. Tang, X. Han, J. Shang, Y. Liu, R.-W. Li, *Adv. Mater. Technol.* **2020**, *5*, 1900934.
[110] J. Chen, H. Liu, W. Wang, N. Nabulsi, W. Zhao, J. Y. Kim, M.-K. Kwon, J.-H. Ryou, *Adv. Funct. Mater.* **2019**, *29*, 1903162.
[111] D. Lee, H. Lee, Y. Jeong, Y. Ahn, G. Nam, Y. Lee, *Adv. Mater.* **2016**, *28*, 9364.
[112] J. G. Simmons, *J. Appl. Phys.* **1963**, *34*, 1793.
[113] M. Chen, K. Li, G. M. Cheng, K. He, W. W. Li, D. S. Zhang, W. M. Li, Y. Feng, L. Wei, W. J. Li, G. H. Zhong, C. L. Yang, *ACS Appl. Mater. Interfaces* **2019**, *11*, 2551.
[114] Y. Zhang, Y. G. Hu, P. L. Zhu, F. Han, Y. Zhu, R. Sun, C. P. Wong, *ACS Appl. Mater. Interfaces* **2017**, *9*, 35968.
[115] Z. Wang, S. Wang, J. Zeng, X. Ren, A. J. Chee, B. Y. Yiu, W. C. Chung, Y. Yang, A. C. Yu, R. C. Roberts, *Small* **2016**, *12*, 3827.

[116] S. Peng, P. Blanloeuil, S. Wu, C. H. Wang, *Adv. Mater. Interf.* **2018**, *5*, 1800403.
[117] X. Wang, L. Dong, H. Zhang, R. Yu, C. Pan, Z. L. Wang, *Adv. Sci.* **2015**, *2*, 1500169.
[118] A. Chhetry, J. Kim, H. Yoon, J. Y. Park, *ACS Appl. Mater. Interfaces* **2019**, *11*, 3438.
[119] Y.-C. Huang, Y. Liu, C. Ma, H.-C. Cheng, Q. He, H. Wu, C. Wang, C.-Y. Lin, Y. Huang, X. Duan, *Nat. Electron.* **2020**, *3*, 59.
[120] H. Park, Y. R. Jeong, J. Yun, S. Y. Hong, S. Jin, S. J. Lee, G. Zi, J. S. Ha, *ACS Nano* **2015**, *9*, 9974.
[121] S. H. Park, H. B. Lee, S. M. Yeon, J. Park, N. K. Lee, *ACS Appl. Mater. Interfaces* **2016**, *8*, 24773.
[122] C. M. Lochner, Y. Khan, A. Pierre, A. C. Arias, *Nat. Commun.* **2014**, *5*.
[123] T. Yokota, P. Zalar, M. Kaltenbrunner, H. Jinno, N. Matsuhisa, H. Kitanosako, Y. Tachibana, W. Yukita, M. Koizumi, T. Someya, *Sci. Adv.* **2016**, *2*, e1501856.
[124] H. Lee, E. Kim, Y. Lee, H. Kim, J. Lee, M. Kim, H.-J. Yoo, S. Yoo, *Sci. Adv.* **2018**, *4*, eaas9530.
[125] M. Nitzan, A. Romem, R. Koppel, *Med. Devices (Auckl)* **2014**, *7*, 231.
[126] H. Pälve, *J. Clin. Monit.* **1992**, *8*, 12.
[127] J. Kim, G. A. Salvatore, H. Araki, A. M. Chiarelli, Z. Xie, A. Banks, X. Sheng, Y. Liu, J. W. Lee, K.-I. Jang, S. Y. Heo, K. Cho, H. Luo, B. Zimmerman, J. Kim, L. Yan, X. Feng, S. Xu, M. Fabiani, G. Gratton, Y. Huang, U. Paik, J. A. Rogers, *Sci. Adv.* **2016**, *2*, e1600418.
[128] Y. Khan, D. Han, A. Pierre, J. Ting, X. Wang, C. M. Lochner, G. Bovo, N. Yaacobi-Gross, C. Newsome, R. Wilson, A. C. Arias, *Proc. Natl. Acad. Sci. USA* **2018**, *115*, E11015.
[129] J. Kim, P. Gutruf, A. M. Chiarelli, S. Y. Heo, K. Cho, Z. Q. Xie, A. Banks, S. Han, K. I. Jang, J. W. Lee, K. T. Lee, X. Feng, Y. G. Huang, M. Fabiani, G. Gratton, U. Paik, J. A. Rogers, *Adv. Funct. Mater.* **2017**, *27*.
[130] H. Jin, Y. S. Abu-Raya, H. Haick, *Adv. Healthcare Mater.* **2017**, *6*, 1700024.
[131] F. Ershad, K. Sim, A. Thukral, Y. S. Zhang, C. Yu, *APL Mater.* **2019**, *7*, 031301.
[132] S. Fokkenrood, P. Leijdekkers, V. Gay, presented at Pervasive Computing for Quality of Life Enhancement, Nara, Japan, June **2007**.
[133] A. Oswal, P. Brown, V. Litvak, *Curr. Opin. Neurol.* **2013**, *26*, 662.
[134] R. M. Rothschild, *Front. Neuroeng.* **2010**, *3*, 112.
[135] J. Gonzalez-Vargas, S. Dosen, S. Amsuess, W. Yu, D. Farina, *PLoS One.* **2015**, *10*, e0127528.
[136] A. Searle, L. Kirkup, *Physiol. Meas.* **2000**, *21*, 271.
[137] E. Huigen, A. Peper, C. A. Grimbergen, *Med. Biol. Eng. Comput.* **2002**, *40*, 332.
[138] A. Zucca, K. Yamagishi, T. Fujie, S. Takeoka, V. Mattoli, F. Greco, *J. Mater. Chem. C* **2015**, *3*, 6539.
[139] J. H. Kim, S. R. Kim, H. J. Kil, Y. C. Kim, J. W. Park, *Nano Lett.* **2018**, *18*, 4531.
[140] S. M. Lee, H. J. Byeon, J. H. Lee, D. H. Baek, K. H. Lee, J. S. Hong, S.-H. Lee, *Sci. Rep.* **2014**, *4*, 6074.
[141] C. Lin, L. Liao, Y. Liu, I. Wang, B. Lin, J. Chang, *IEEE Trans. Biomed. Eng.* **2011**, *58*, 1200.
[142] F. Stauffer, M. Thielen, C. Sauter, S. Chardonnens, S. Bachmann, K. Tybrandt, C. Peters, C. Hierold, J. Vörös, *Adv. Healthcare Mater.* **2018**, *7*, 1700994.
[143] S. Chun, D. W. Kim, S. Baik, H. J. Lee, J. H. Lee, S. H. Bhang, C. Pang, *Adv. Funct. Mater.* **2018**, *28*, 1805224.
[144] J. Moyer, D. Wilson, I. Finkelshtein, B. Wong, R. Potts, *Diabetes Technol. Ther.* **2012**, *14*, 398.

[145] J. Kim, I. Jeerapan, S. Imani, T. N. Cho, A. Bandodkar, S. Cinti, P. P. Mercier, J. Wang, *ACS Sens.* **2016**, *1*, 1011.
[146] H. Y. Y. Nyein, W. Gao, Z. Shahpar, S. Emaminejad, S. Challa, K. Chen, H. M. Fahad, L. C. Tai, H. Ota, R. W. Davis, A. Javey, *ACS Nano* **2016**, *10*, 7216.
[147] H. Lee, T. K. Choi, Y. B. Lee, H. R. Cho, R. Ghaffari, L. Wang, H. J. Choi, T. D. Chung, N. Lu, T. Hyeon, S. H. Choi, D.-H. Kim, *Nat. Nanotechnol.* **2016**, *11*, 566.
[148] H. Lee, Y. J. Hong, S. Baik, T. Hyeon, D.-H. Kim, *Adv. Healthcare Mater.* **2018**, *7*, 1701150.
[149] L.-C. Tai, W. Gao, M. Chao, M. Bariya, Q. P. Ngo, Z. Shahpar, H. Y. Y. Nyein, H. Park, J. Sun, Y. Jung, E. Wu, H. M. Fahad, D.-H. Lien, H. Ota, G. Cho, A. Javey, *Adv. Mater.* **2018**, *30*, 1707442.
[150] R. Ghaffari, J. Choi, M. S. Raj, S. Chen, S. P. Lee, J. T. Reeder, A. J. Aranyosi, A. Leech, W. Li, S. Schon, J. B. Model, J. A. Rogers, *Adv. Funct. Mater.* **2019**, *n/a*, 1907269.
[151] M. C. Brothers, M. DeBrosse, C. C. Grigsby, R. R. Naik, S. M. Hussain, J. Heikenfeld, S. S. Kim, *Acc. Chem. Res.* **2019**, *52*, 297.
[152] Y. Cui, L. Zhang, M. Zhang, X. Yang, L. Zhang, J. Kuang, G. Zhang, Q. Liu, H. Guo, Q. Meng, *Sci. Rep.* **2017**, *7*, 11195.
[153] Y. Zhang, H. Guo, S. B. Kim, Y. Wu, D. Ostojich, S. H. Park, X. Wang, Z. Weng, R. Li, A. J. Bandodkar, Y. Sekine, J. Choi, S. Xu, S. Quaggin, R. Ghaffari, J. A. Rogers, *Lab on a Chip* **2019**, *19*, 1545.
[154] O. Parlak, S. T. Keene, A. Marais, V. F. Curto, A. Salleo, *Sci. Adv.* **2018**, *4*, eaar2904.
[155] J. Choi, A. J. Bandodkar, J. T. Reeder, T. R. Ray, A. Turnquist, S. B. Kim, N. Nyberg, A. Hourlier-Fargette, J. B. Model, A. J. Aranyosi, S. Xu, R. Ghaffari, J. A. Rogers, *ACS Sens.* **2019**, *4*, 379.
[156] A. J. Bandodkar, P. Gutruf, J. Choi, K. Lee, Y. Sekine, J. T. Reeder, W. J. Jeang, A. J. Aranyosi, S. P. Lee, J. B. Model, R. Ghaffari, C.-J. Su, J. P. Leshock, T. Ray, A. Verrillo, K. Thomas, V. Krishnamurthi, S. Han, J. Kim, S. Krishnan, T. Hang, J. A. Rogers, *Sci. Adv.* **2019**, *5*, eaav3294.
[157] M. Bariya, H. Y. Y. Nyein, A. Javey, *Nat. Electron.* **2018**, *1*, 160.
[158] S. Nakata, M. Shiomi, Y. Fujita, T. Arie, S. Akita, K. Takei, *Nat. Electron.* **2018**, *1*, 596.
[159] A. Bhide, S. Muthukumar, A. Saini, S. Prasad, *Sci. Rep.* **2018**, *8*, 6507.
[160] J. Choi, R. Ghaffari, L. B. Baker, J. A. Rogers, *Sci. Adv.* **2018**, *4*, eaar3921.
[161] P. Si, Y. Huang, T. Wang, J. Ma, *RSC Adv.* **2013**, *3*, 3487.
[162] S. Y. Oh, S. Y. Hong, Y. R. Jeong, J. Yun, H. Park, S. W. Jin, G. Lee, J. H. Oh, H. Lee, S. S. Lee, J. S. Ha, *ACS Appl. Mater. Interfaces* **2018**, *10*, 13729.
[163] A. Koh, D. Kang, Y. Xue, S. Lee, R. M. Pielak, J. Kim, T. Hwang, S. Min, A. Banks, P. Bastien, M. C. Manco, L. Wang, K. R. Ammann, K.-I. Jang, P. Won, S. Han, R. Ghaffari, U. Paik, M. J. Slepian, G. Balooch, Y. Huang, J. A. Rogers, *Sci. Transl. Med.* **2016**, *8*, 366ra165.
[164] A. Martin, J. Kim, J. F. Kurniawan, J. R. Sempionatto, J. R. Moreto, G. D. Tang, A. S. Campbell, A. Shin, M. Y. Lee, X. F. Liu, J. Wang, *ACS Sens.* **2017**, *2*, 1860.
[165] T. A. Kuiken, G. Li, B. A. Lock, R. D. Lipschutz, L. A. Miller, K. A. Stubblefield, K. B. Englehart, *JAMA* **2009**, *301*, 619.
[166] T. A. Kuiken, P. D. Marasco, B. A. Lock, R. N. Harden, J. P. A. Dewald, *Proc. Natl. Acad. Sci. USA* **2007**, *104*, 20061.
[167] B. Peerdeman, D. Boere, H. Witteveen, R. Huis in `tVeld, H. Hermens, S. Stramigioli, H. Rietman, P. Veltink, S. Misra, *J. Rehabil. Res. Dev.* **2011**, *48*, 719.
[168] T. Chen, Q. Shi, M. Zhu, T. He, L. Sun, L. Yang, C. Lee, *ACS Nano* **2018**, *12*, 11561.

[169] S. Lim, D. Son, J. Kim, Y. B. Lee, J.-K. Song, S. Choi, D. J. Lee, J. H. Kim, M. Lee, T. Hyeon, D.-H. Kim, *Adv. Funct. Mater.* **2015**, *25*, 375.
[170] J. Byun, Y. Lee, J. Yoon, B. Lee, E. Oh, S. Chung, T. Lee, K.-J. Cho, J. Kim, Y. Hong, *Sci. Robot.* **2018**, *3*, eaas9020.
[171] I. N. Kholmanov, C. W. Magnuson, A. E. Aliev, H. Li, B. Zhang, J. W. Suk, L. L. Zhang, E. Peng, S. H. Mousavi, A. B. Khanikaev, R. Piner, G. Shvets, R. S. Ruoff, *Nano Lett.* **2012**, *12*, 5679.
[172] B. Xu, A. Akhtar, Y. Liu, H. Chen, W.-H. Yeo, S. Park, II, B. Boyce, H. Kim, J. Yu, H.-Y. Lai, S. Jung, Y. Zhou, J. Kim, S. Cho, Y. Huang, T. Bretl, J. A. Rogers, *Adv. Mater.* **2016**, *28*, 4462.
[173] X. Pu, H. Guo, J. Chen, X. Wang, Y. Xi, C. Hu, Z. L. Wang, *Sci. Adv.* **2017**, *3*, e1700694.
[174] R. D. P. Wong, J. D. Posner, V. J. Santos, *Sens. Actuat. A-Phys.* **2012**, *179*, 62.
[175] Y. Tang, H. Zhou, X. Sun, N. Diao, J. Wang, B. Zhang, C. Qin, E. Liang, Y. Mao, *Adv. Funct. Mater.* **2020**, *30*, 1907893.
[176] B. Zhang, Y. Tang, R. Dai, H. Wang, X. Sun, C. Qin, Z. Pan, E. Liang, Y. Mao, *Nano Energy* **2019**, *64*, 103953.
[177] J. Yang, R. Shi, Z. Lou, R. Chai, K. Jiang, G. Shen, *Small* **2019**, *15*, 1902801.
[178] R. Cao, X. Pu, X. Du, W. Yang, J. Wang, H. Guo, S. Zhao, Z. Yuan, C. Zhang, C. Li, Z. L. Wang, *ACS Nano* **2018**, *12*, 5190.
[179] J. Tao, R. Bao, X. Wang, Y. Peng, J. Li, S. Fu, C. Pan, Z. L. Wang, *Adv. Funct. Mater.* **2019**, *29*, 1806379.
[180] S. Jung, J. H. Kim, J. Kim, S. Choi, J. Lee, I. Park, T. Hyeon, D.-H. Kim, *Adv. Mater.* **2014**, *26*, 4825.
[181] Q. Shi, C. Lee, *Adv. Sci.* **2019**, *6*, 1900617.
[182] S. Mishra, J. J. S. Norton, Y. Lee, D. S. Lee, N. Agee, Y. Chen, Y. Chun, W.-H. Yeo, *Biosens. Bioelectron.* **2017**, *91*, 796.
[183] S. K. Ameri, M. Kim, I. A. Kuang, W. K. Perera, M. Alshiekh, H. Jeong, U. Topcu, D. Akinwande, N. Lu, *NPJ 2D Mater. Appl.* **2018**, *2*, 19.
[184] C.-C. Kim, H.-H. Lee, K. H. Oh, J.-Y. Sun, *Science* **2016**, *353*, 682.
[185] S. Takamatsu, T. Lonjaret, E. Ismailova, A. Masuda, T. Itoh, G. G. Malliaras, *Adv. Mater.* **2016**, *28*, 4485.
[186] T. He, Z. Sun, Q. Shi, M. Zhu, D. V. Anaya, M. Xu, T. Chen, M. R. Yuce, A. V.-Y. Thean, C. Lee, *Nano Energy* **2019**, *58*, 641.
[187] J. J. S. Norton, D. S. Lee, J. W. Lee, W. Lee, O. Kwon, P. Won, S.-Y. Jung, H. Cheng, J.-W. Jeong, A. Akce, S. Umunna, I. Na, Y. H. Kwon, X.-Q. Wang, Z. Liu, U. Paik, Y. Huang, T. Bretl, W.-H. Yeo, J. A. Rogers, *Proc. Natl. Acad. Sci. USA* **2015**, *112*, 3920.
[188] Y. Liu, J. J. S. Norton, R. Qazi, Z. Zou, K. R. Ammann, H. Liu, L. Yan, P. L. Tran, K.-I. Jang, J. W. Lee, D. Zhang, K. A. Kilian, S. H. Jung, T. Bretl, J. Xiao, M. J. Slepian, Y. Huang, J.-W. Jeong, J. A. Rogers, *Sci. Adv.* **2016**, *2*, e1601185.
[189] M. M. Müller, S. Hillyard, *Clin. Neurophysiol.* **2000**, *111*, 1544.
[190] Y. Guo, M. Zhong, Z. Fang, P. Wan, G. Yu, *Nano Lett.* **2019**, *19*, 1143.
[191] X. Liao, W. Song, X. Zhang, H. Huang, Y. Wang, Y. Zheng, *J. Mater. Chem. C* **2018**, *6*, 12841.
[192] H. Wang, X. Ma, Y. Hao, *Adv. Mater. Interf.* **2017**, *4*, 1600709.
[193] I. del Agua, D. Mantione, U. Ismailov, A. Sanchez-Sanchez, N. Aramburu, G. G. Malliaras, D. Mecerreyes, E. Ismailova, *Adv. Mater. Technol.* **2018**, *3*, 1700322.
[194] S. Choi, S. I. Han, D. Jung, H. J. Hwang, C. Lim, S. Bae, O. K. Park, C. M. Tschabrunn, M. Lee, S. Y. Bae, J. W. Yu, J. H. Ryu, S.-W. Lee, K. Park, P. M. Kang, W. B. Lee, R. Nezafat, T. Hyeon, D.-H. Kim, *Nat. Nanotechnol.* **2018**, *13*, 1048.
[195] S. Gong, W. Cheng, *Adv. Electron. Mater.* **2017**, *7*, 1700648.

[196] L. Li, H. Xiang, Y. Xiong, H. Zhao, Y. Bai, S. Wang, F. Sun, M. Hao, L. Liu, T. Li, Z. Peng, J. Xu, T. Zhang, *Adv. Sci.* **2018**, *5*, 1800558.
[197] M. A. Parvez Mahmud, N. Huda, S. H. Farjana, M. Asadnia, C. Lang, *Adv. Electron. Mater.* **2018**, *8*, 1701210.
[198] D.-H. Kim, R. Ghaffari, N. Lu, S. Wang, S. P. Lee, H. Keum, R. D'Angelo, L. Klinker, Y. Su, C. Lu, Y.-S. Kim, A. Ameen, Y. Li, Y. Zhang, B. de Graff, Y.-Y. Hsu, Z. Liu, J. Ruskin, L. Xu, C. Lu, F. G. Omenetto, Y. Huang, M. Mansour, M. J. Slepian, J. A. Rogers, *Proc. Natl. Acad. Sci. USA* **2012**, *109*, 19910.
[199] L. Xu, S. R. Gutbrod, A. P. Bonifas, Y. Su, M. S. Sulkin, N. Lu, H.-J. Chung, K.-I. Jang, Z. Liu, M. Ying, C. Lu, R. C. Webb, J.-S. Kim, J. I. Laughner, H. Cheng, Y. Liu, A. Ameen, J.-W. Jeong, G.-T. Kim, Y. Huang, I. R. Efimov, J. A. Rogers, *Nat. Commun.* **2014**, *5*, 3329.
[200] H. Chen, L. Bai, T. Li, C. Zhao, J. Zhang, N. Zhang, G. Song, Q. Gan, Y. Xu, *Nano Energy* **2018**, *46*, 73.
[201] A. Kumar, *Manufacturing Letters* **2018**, *15*, 122.
[202] J. Park, J. Kim, K. Kim, S.-Y. Kim, W. H. Cheong, K. Park, J. H. Song, G. Namgoong, J. J. Kim, J. Heo, F. Bien, J.-U. Park, *Nanoscale* **2016**, *8*, 10591.
[203] A. Shamim, M. Vaseem, A. Sizhe, M. F. Farooqui, presented at 2018 International Flexible Electronics Technology Conference (IFETC), Ottawa, Canada, Aug. **2018**.
[204] A. Chortos, J. Liu, Z. Bao, *Nat. Mater.* **2016**, *15*, 937.
[205] J. Ge, L. Sun, F.-R. Zhang, Y. Zhang, L.-A. Shi, H.-Y. Zhao, H.-W. Zhu, H.-L. Jiang, S.-H. Yu, *Adv. Mater.* **2016**, *28*, 722.
[206] S. Han, M. K. Kim, B. Wang, D. S. Wie, S. Wang, C. H. Lee, *Adv. Mater.* **2016**, *28*, 10257.
[207] Y. Song, W. Huang, C. Mu, X. Chen, Q. Zhang, A. Ran, Z. Peng, R. Sun, W. Xie, *Adv. Mater. Technol.* **2019**, *4*, 1800680.

Figures

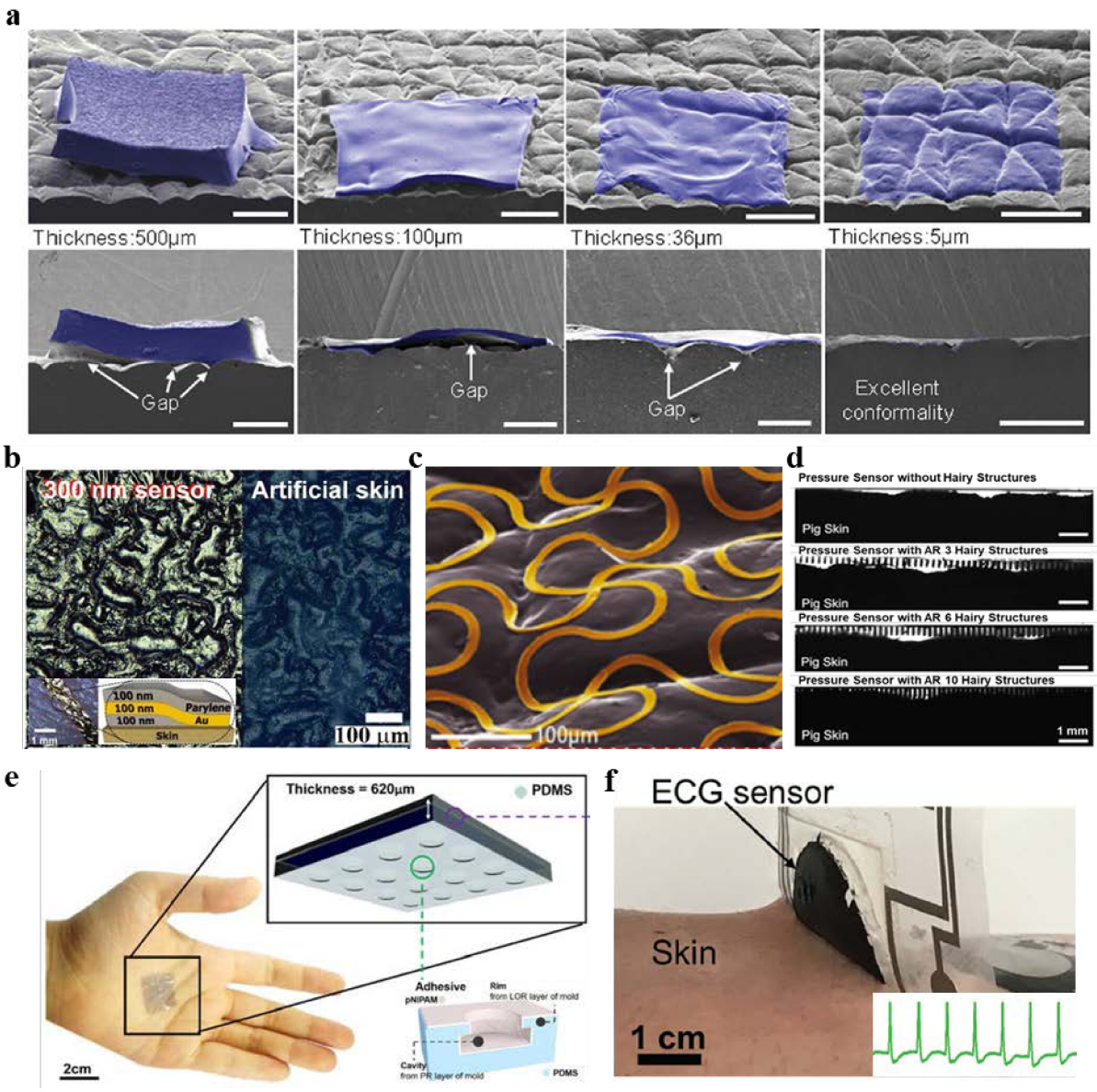

Figure 1. Strategies to interface soft electronics with skin. a) Angled and cross-sectional SEM images showing the degree of conformal contact between skin replica (grey) and elastomer membrane substrates with various thicknesses (blue). Reproduced with permission.[70] Copyright 2013, Wiley-VCH. b) Ultra-thin self-adhesive film on the skin. Reproduced with permission.[67] Copyright 2018, Wiley-VCH. c) Magnified view of the colorized SEM image of epidermal electronics mounted on the skin replica. Reproduced with permission.[72] Copyright 2013, Wiley-VCH. d) Cross-sectional profiles of PDMS microhair structures with

various aspect ratios on a pig skin under pressure. Adapted with permission.[73] Copyright 2015, Wiley-VCH. e) Schematic illustration of the self-adhesive temperature sensor with a microstructured PDMS adhesive attached by suction on the palm. Adapted with permission.[74] Copyright 2018, American Chemical Society. f) The self-adhesive PDMS strain sensor prepared by mixing the curing inhibitor and conductive CNT. Reproduced with permission.[75] Copyright 2016, Wiley-VCH.

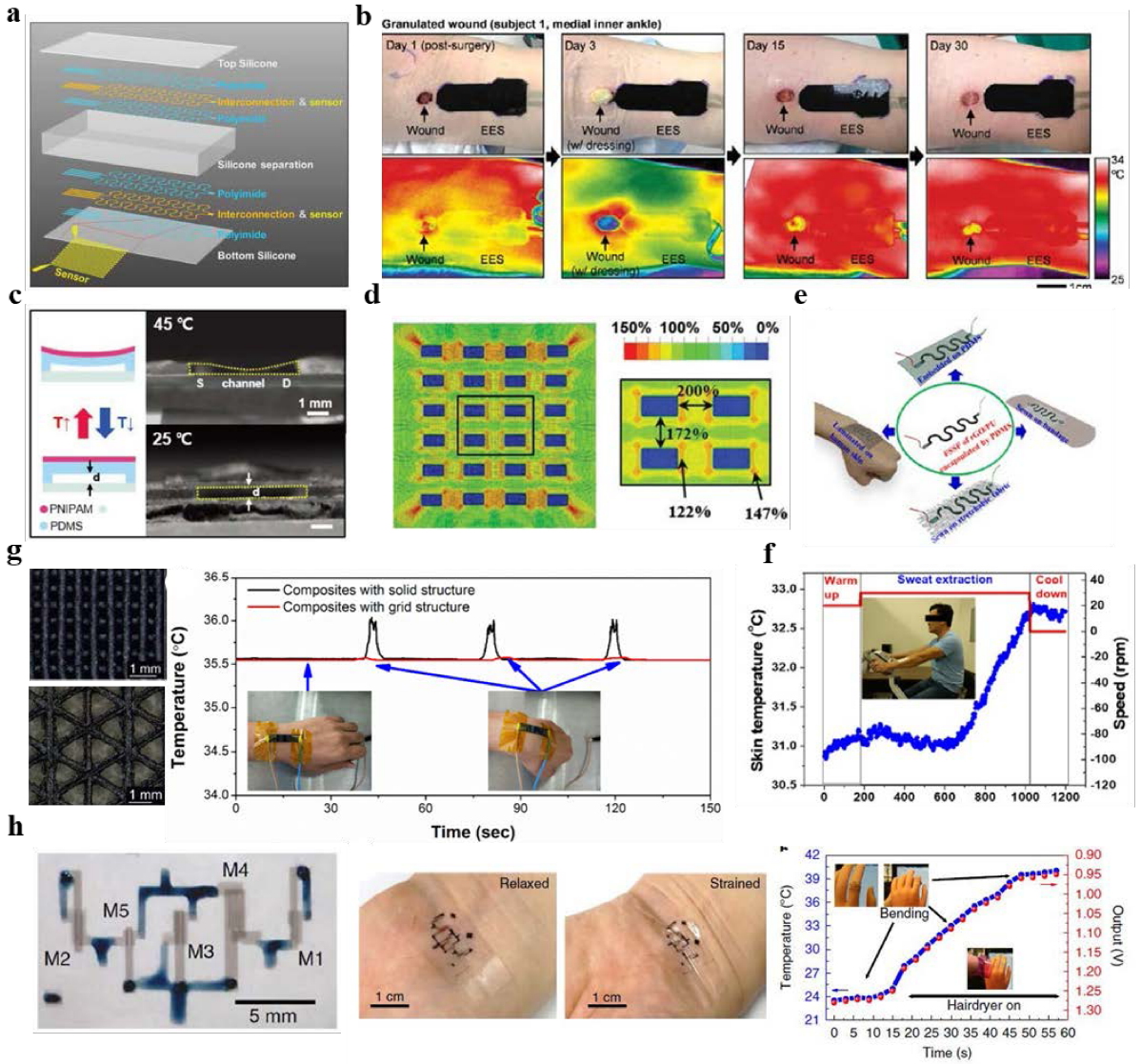

Figure 2. Soft temperature sensors. a) Schematic illustration of the ultrathin and filamentary serpentine gold-based temperature sensors. Reproduced with permission.[84] Copyright 2016, Wiley-VCH. b) Epidermal electronics system including temperature sensors near a granulated wound. The photos of the wound on day 1 to day 30 (top row), and corresponding IR images of the temperature distribution (bottom row). Reproduced with permission.[83] Copyright 2014, Wiley-VCH. c) Schematic image (left) and optical image (right) of a temperature sensitive PNIPAM suspended on top of the channel, where the air-gap distance is controlled by the temperature change. Reproduced with permission.[86] Copyright 2018, Wiley-VCH. d) FEM analysis of a stretchable temperature sensor array in a strain island structure under biaxial

stretching of 50%. Reproduced with permission.[86] Copyright 2018, Wiley-VCH. e) Schematic diagram showing the strain insensitive temperature sensor with a serpentine layout. f) The stretchable temperature sensor on a bandage accurately measured the temperature of the forearm (inset) during cycling. Reproduced with permission.[98] Copyright 2018, American Chemical Society. g) Optical images of the 3D-printed graphene/PDMS composites with grid structures and triangular porous structures (left). Simultaneous temperature monitoring of the skin temperature on the wrist during bending of stretchable and non-stretchable temperature sensors (right). Reproduced with permission.[85] Copyright 2019, American Chemical Society. h) Stretchable strain insensitive temperature-sensing circuit with differential voltage read-out. Reproduced with permission. [99] Copyright 2019, Springer Nature.

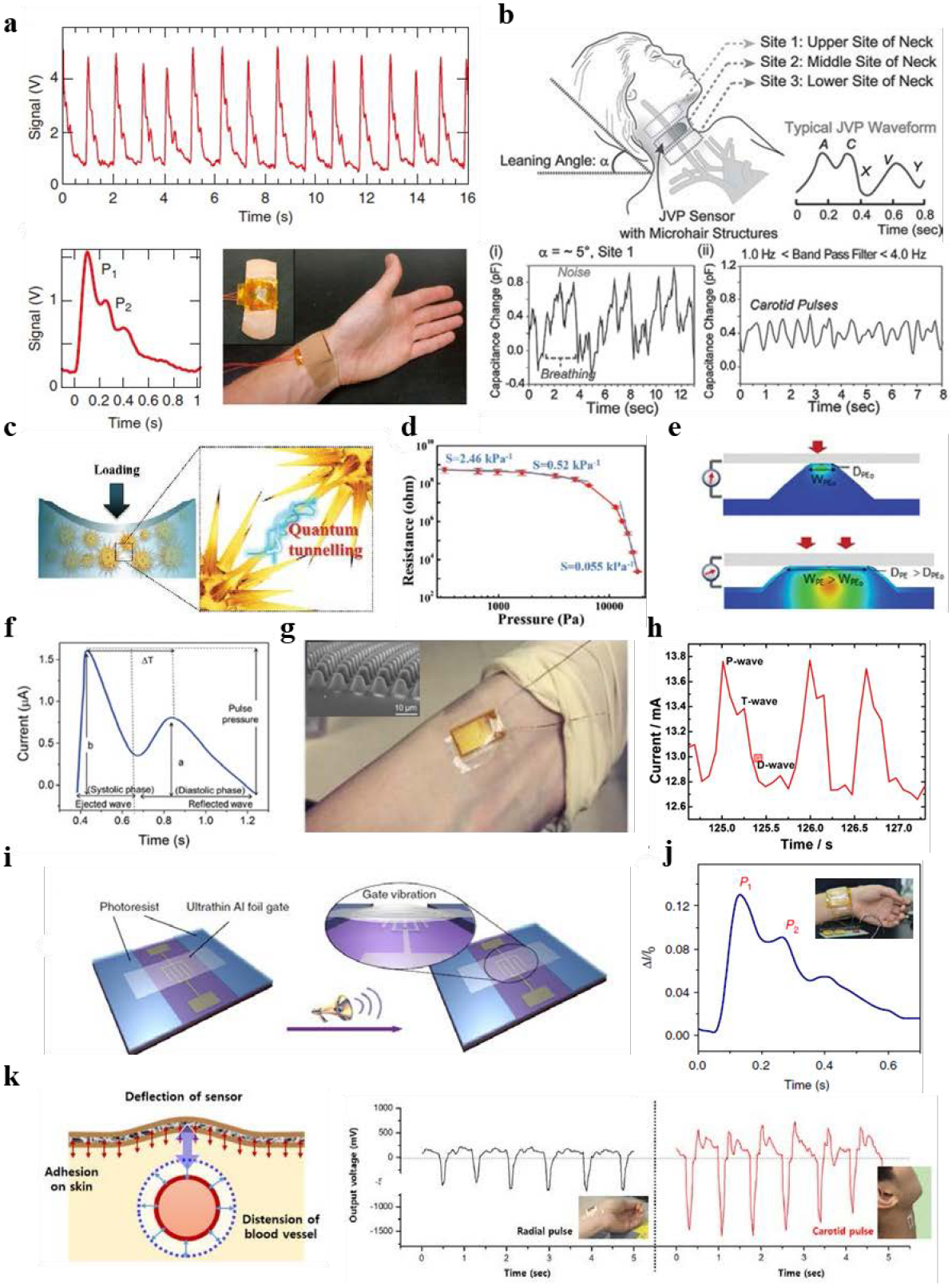

Figure 3. Soft pressure sensors for pulses monitoring. a) Flexible pressure-sensitive FET on an adult human wrist radial artery monitoring the blood pressure in real time. Reproduced with permission.[103] Copyright 2013, Springer Nature. b) Schematic illustration of the jugular

venous pulse (JVP) measured on the human subject's neck using a microhair-structured pressure sensor at three different sites (top). Capacitive response and corresponding carotid pulse and JVP at site 1 from a healthy person. Reproduced with permission.[73] Copyright 2014, Wiley-VCH. c, d) Mechanism of the piezoresistive sea urchin-shaped metal nanoparticles /PU composite with a sensitivity as high as 2.46 kPa^{-1}. Reproduced with permission.[111] Copyright 2016, Wiley-VCH. e) Schematic mechanism of the piezoresistive pressure sensors with the micropyramid structured PDMS, and f) pulse waveform showing clear systolic and diastolic peaks. Reproduced with permission.[104] Copyright 2014, Wiley-VCH. g) Pressure sensor with the conical frustum-like PDMS microstructures (inset) on human wrist and h) real-time waveform of arterial pulses. Reproduced with permission.[113] Copyright 2018, American Chemical Society. i) Schematic illustration of the pressure sensitive FET and j) a detailed curve of pulse wave signals: P1, P2, and diastolic wave are observed clearly. Reproduced with permission.[106] Copyright 2015, Springer Nature. k) Schematic illustration of the working mechanism of sensor−skin deflection by arterial distension and pulse wave form detected from the radial and carotid nerves. Reproduced with permission.[121] Copyright 2016, American Chemical Society.

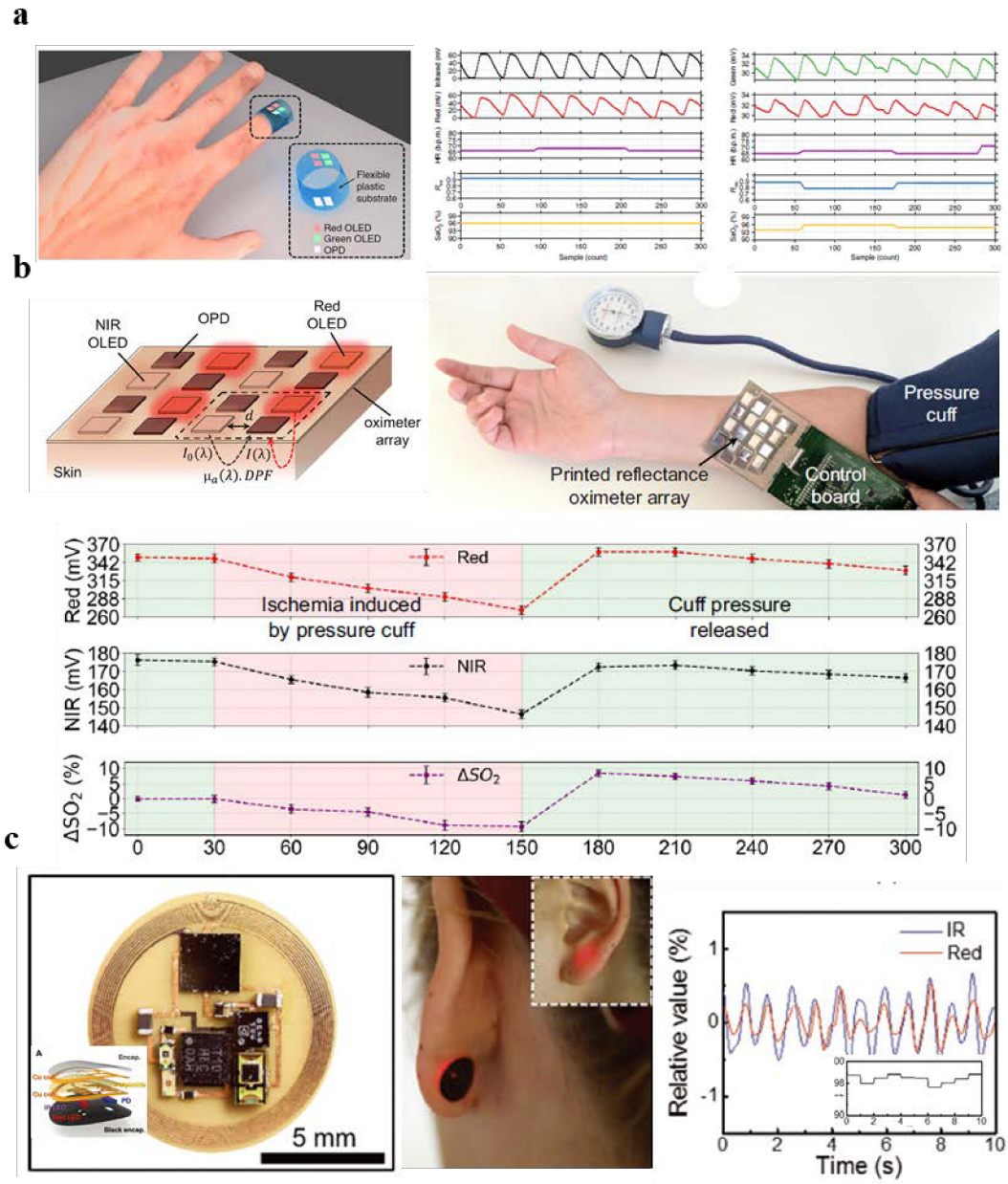

Figure 4. Soft pulse oximeters. a) Flexible transmission pulse oximeter wrapped around a fingertip. The PPG signals were obtained from a commercially available inorganic oximeter probe (middle) and the flexible transmission pulse oximeter (right). Reproduced with permission (right).[122] Copyright 2014, Springer Nature. b) Flexible organic reflectance oximeter array (top left) on the forearm measuring ΔSO_2 under ischemia induced by a pressure cuff (top right) and red, NIR, and ΔSO_2 data with and without ischemia (bottom). Reproduced with permission.[128] Copyright 2014, National Academy of Sciences. c) Image and exploded view (inset) of a wireless pulse oximeter device (left) on the back of the earlobe (middle), and

relative values of the red and IR signals obtained from the earlobe (right). Reproduced with permission.[127, 129] Copyright 2016, Wiley-VCH.

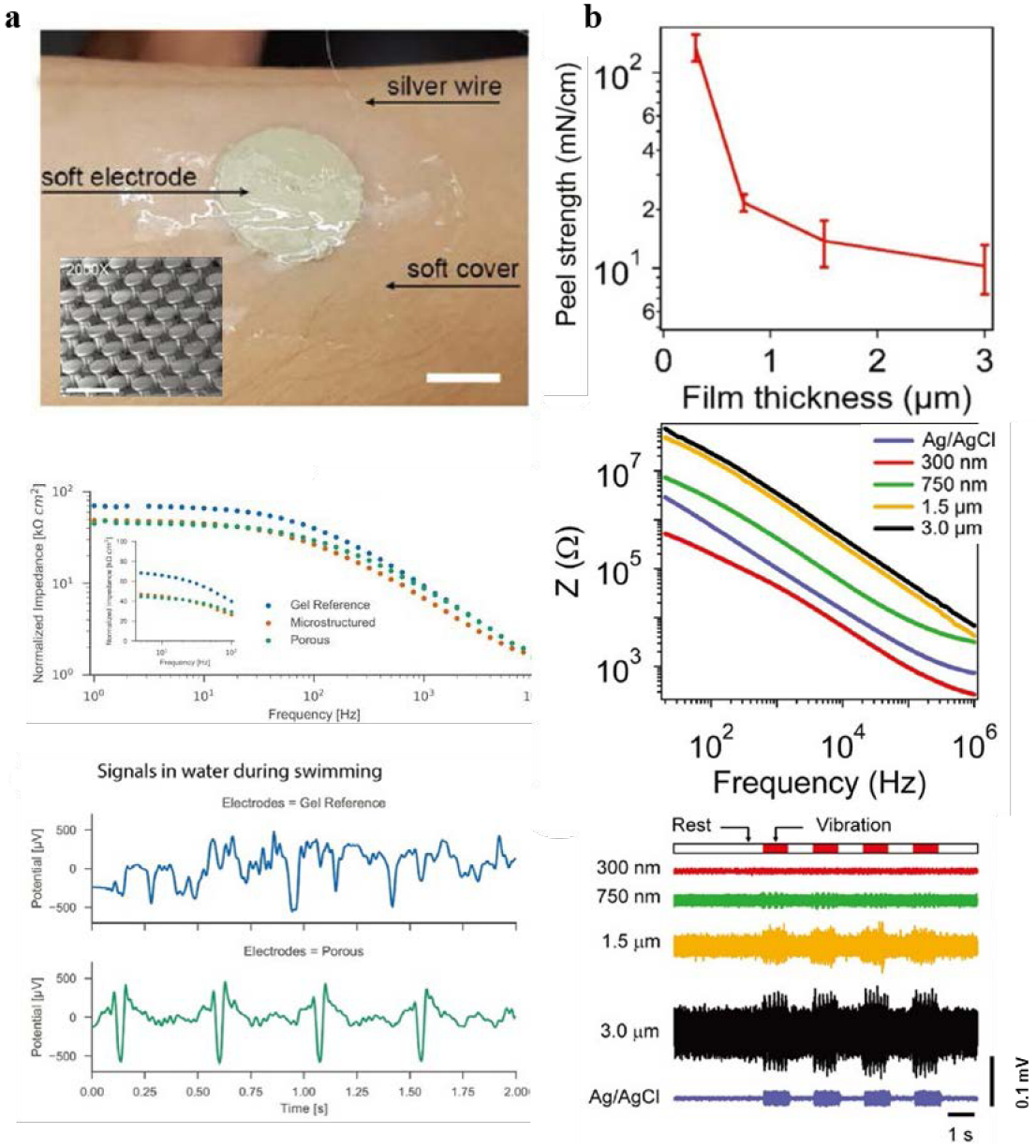

Figure 5. Soft electrophysiological sensors. a) Self-adhesive PDMS electrodes with microstructures and the SEM image of the microstructures (inset). Frequency dependence of normalized electrode-skin impedance of different electrodes (middle). ECG signal recording from gel electrodes and porous electrodes during swimming. Reproduced with permission.[142] Copyright 2018, Wiley-VCH. b) Peel strength of the thin film electrodes of various thicknesses, delaminated from the surface of the artificial skin (top). Impedance of Ag/AgCl and thin film sensors of various thicknesses (middle). Comparison of the EMG noise of thin film sensors of varying thicknesses and a reference Ag/AgCl sensor due to induced skin vibration (bottom).

Reproduced with permission.[67] Copyright 2018, Wiley-VCH.

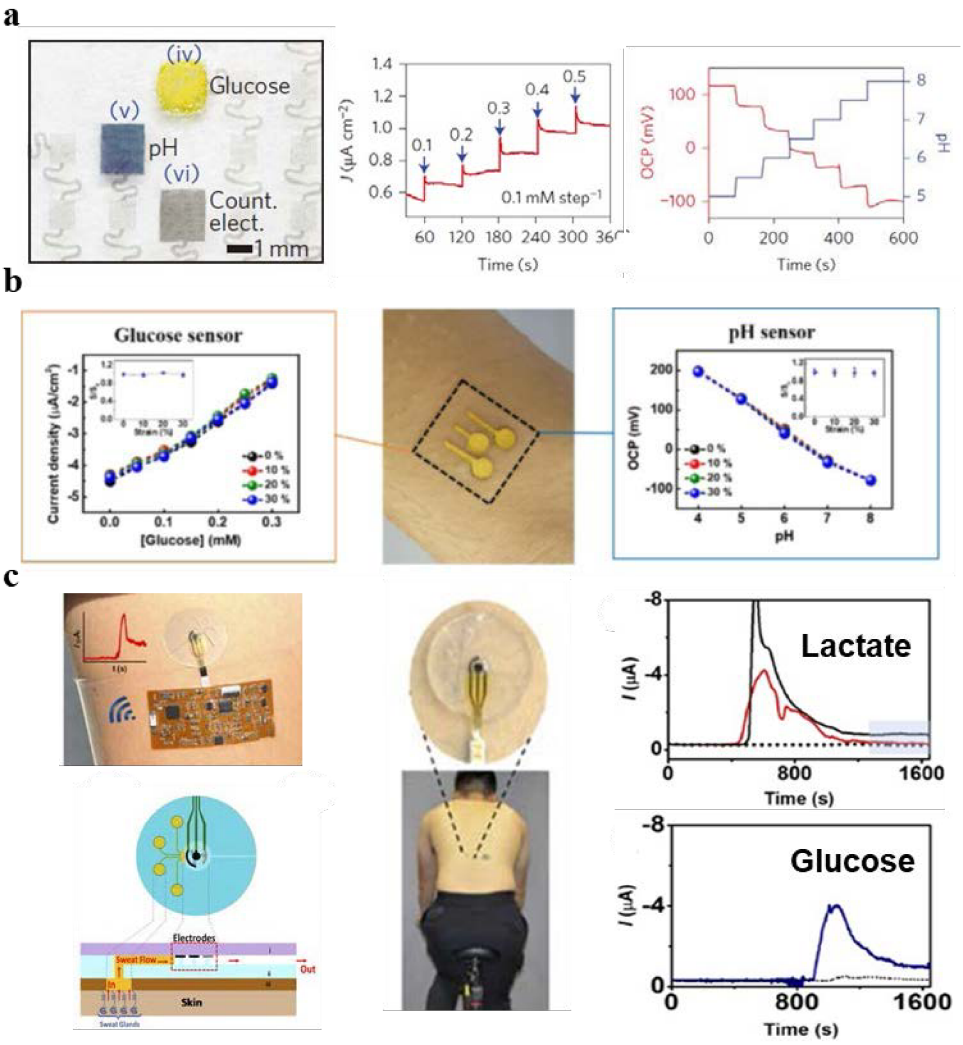

Figure 6. Soft sweat sensors. a) Optical image of stretchable sweat sensor with an Au doped graphene electrode (left), calibration curve of the glucose sensor (middle) and pH sensor (right). Reproduced with permission.[147] Copyright 2016, Springer Nature. b) Photographic image of the electrochemical sensor attached to the skin wet with sweat (middle), and characteristics of the glucose sensor (left) and pH sensor (right) under stretching deformation; insets shows sensitivities at different applied strains. Reproduced with permission.[162] Copyright 2018, American Chemical Society. c) Photograph of the wireless sweat device integrated with microfluidic sweat collection (top left) and schematic representation of sweat collection by the microfluidic channel (bottom left). The wireless sweat device was mounted on the lower back of the subject during cycling (middle), and real-time lactate (top right) and glucose (bottom

right) monitoring. Reproduced with permission.[164] Copyright 2018, American Chemical Society.

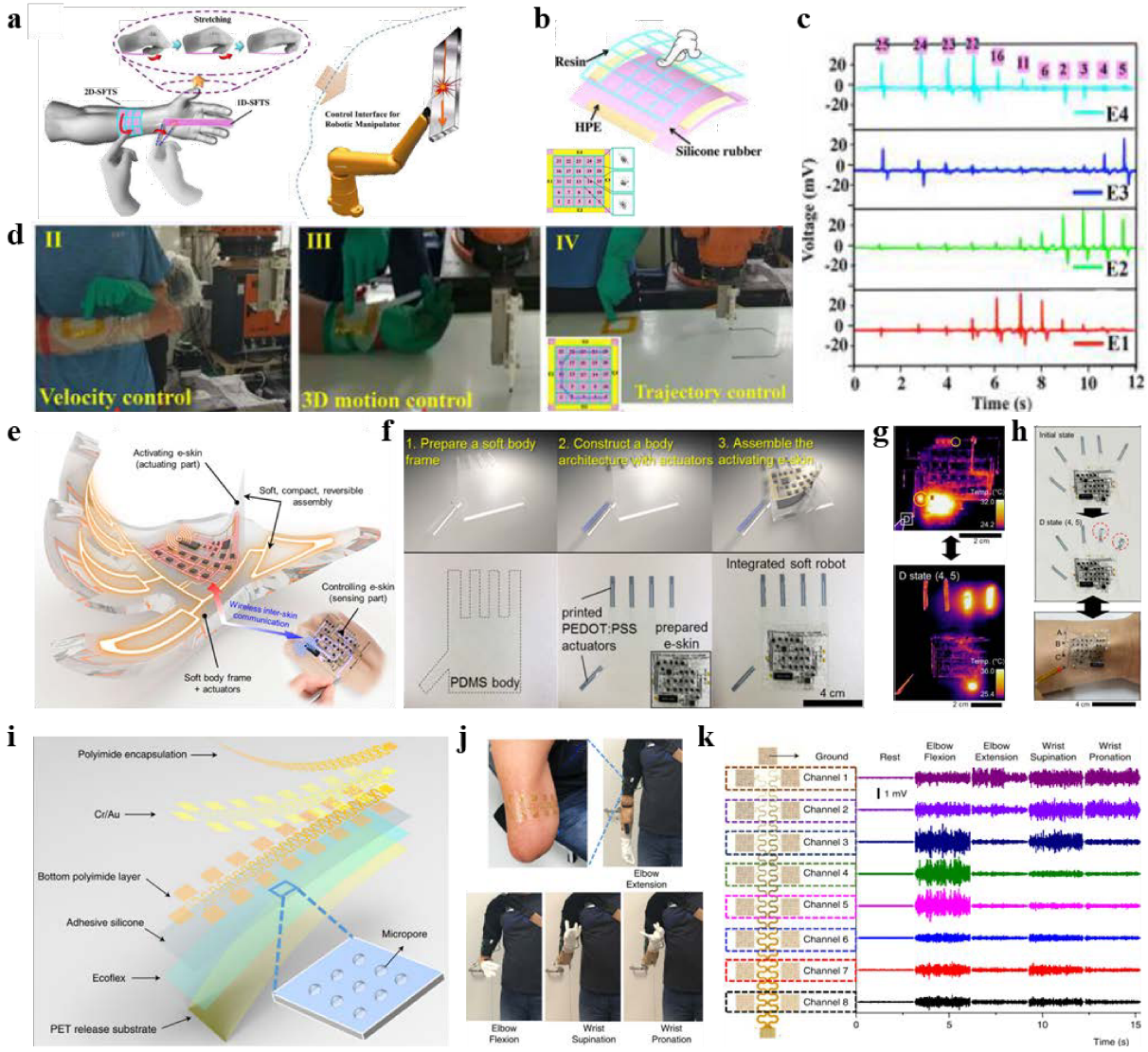

Figure 7. Soft electronics enabled prosthetic limb control. a) Schematic illustration and arrangement of the 2D-SFTS and 1D-SFTS used in tandem to achieve 3D motion control. b) Exploded schematic of the 2D-SFTS. Arrangement of 4 electrodes E1, E2, E3, E4 and the voltage responses at lattices 13, 15, and 25 showing good centrality (inset). c) Voltage response of 4 electrodes during the trajectory control when drawing the letter C. d) Demonstrations of velocity control (left), 3D motion control (middle), and trajectory control (right). The robotic arm was used to draw the letter C. Reproduced with permission.[168] e) Schematic illustration of a soft robotic hand controlled by a control skin worn on a human subject's hand. The skin communicated wirelessly and controlled the soft robot. f) Fabrication and assembly of the soft robotic hand and the control skin. g) Thermographic image (top) of the control skins on the

human wrist and activated state of the robotic hand (bottom). h) Optical images of the initial and activated D state (top) and control skin on human wrist (bottom). i) Exploded schematic view of the large-area epidermal electronics. j) Large EES placed on the amputated upper limb of a subject and various states of the prosthetic arm. k) 8 channels of recorded EMG during the different states of the prosthetic arm. a-d) Reproduced with permission.[168] Copyright 2018, American Chemical Society. e-h) Reproduced with permission.[170] Copyright 2018, American Association for the Advancement of Science. i-k) Reproduced with permission.[80] Copyright 2019, Springer Nature.

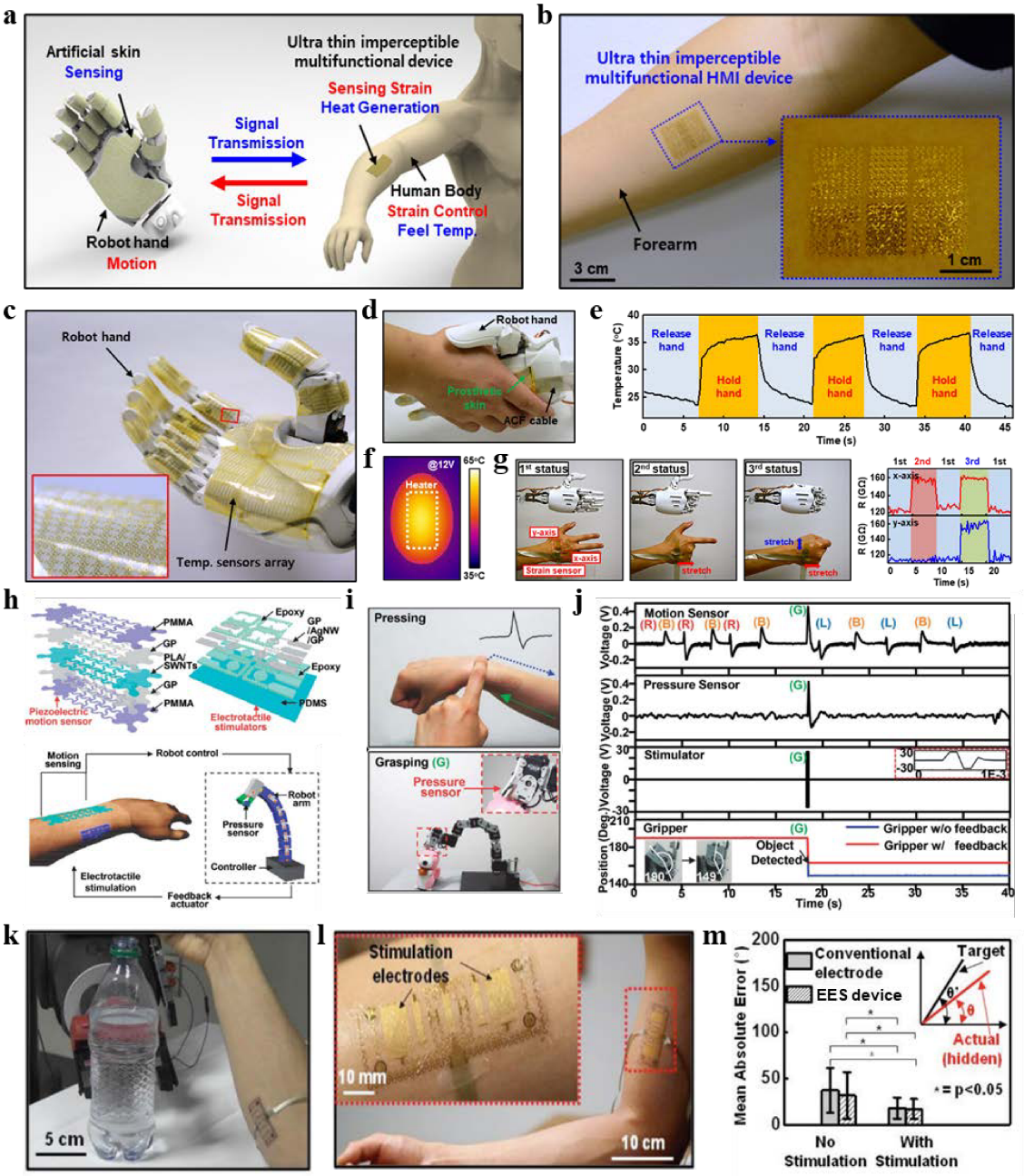

Figure 8. Closed-loop interactive HMIs. a) Schematic showing signal transmission between the artificial skin of the robotic hand and the ultrathin imperceptible multifunctional HMI device on the forearm of a human subject. b) HMI device worn on the forearm. Inset shows the various arrayed devices including resistive random-access memory, field effect transistors, temperature sensors, strain sensors, ultraviolet (UV) sensors, and microheaters. c) Artificial skin of the robotic hand. Inset is a zoomed in view of the temperature sensor array. d) Human subject holding the robotic hand equipped with the artificial skin. e) The resistance change

based on the temperature detected by the robotic hand. f) Infrared camera image of the microheater. g) Strain sensors on the human hand used to control the configuration of the robotic hand. h) Exploded schematic view of the piezoelectric motion sensor (top left) and electrotactile stimulator (top right). Schematic illustration of the closed-loop feedback of the robotic arm with the sensor and stimulator. i) One representative state of human-machine interaction. Pressing on the piezoelectric sensor causes the robotic arm to grasp (G), bending the wrist causes the robotic arm to bend. j) Responses of the human forearm motion sensor, pressure sensor, electrotactile stimulator, and robotic arm pressure sensor under relaxing (R), bending (B), grasping (G), and lifting (L) states. The pressure sensor on the human controls only the grasping ability of the robotic arm. The stimulator delivers a signal and the inset shows zoomed view of the stimulation pulse. Measured positional status of the robotic arm ranging from 149° to 190°, representing completely closed and completely opened states of the arm, respectively. k) EMG sensors placed on the forearm to control the gripping force of the robotic arm. l) EES device worn on the bicep. m) Results of the classification showing comparable performance of the epidermal electronic system (EES) device and conventional electrodes. Schematic illustration of the virtual arm (inset). a-g) Reproduced with permission.[54] Copyright 2019, American Association for the Advancement of Science. h-j) Reproduced with permission.[169] Copyright 2015, Wiley-VCH. k-m) Reproduced with permission.[172] Copyright 2016, Wiley-VCH.

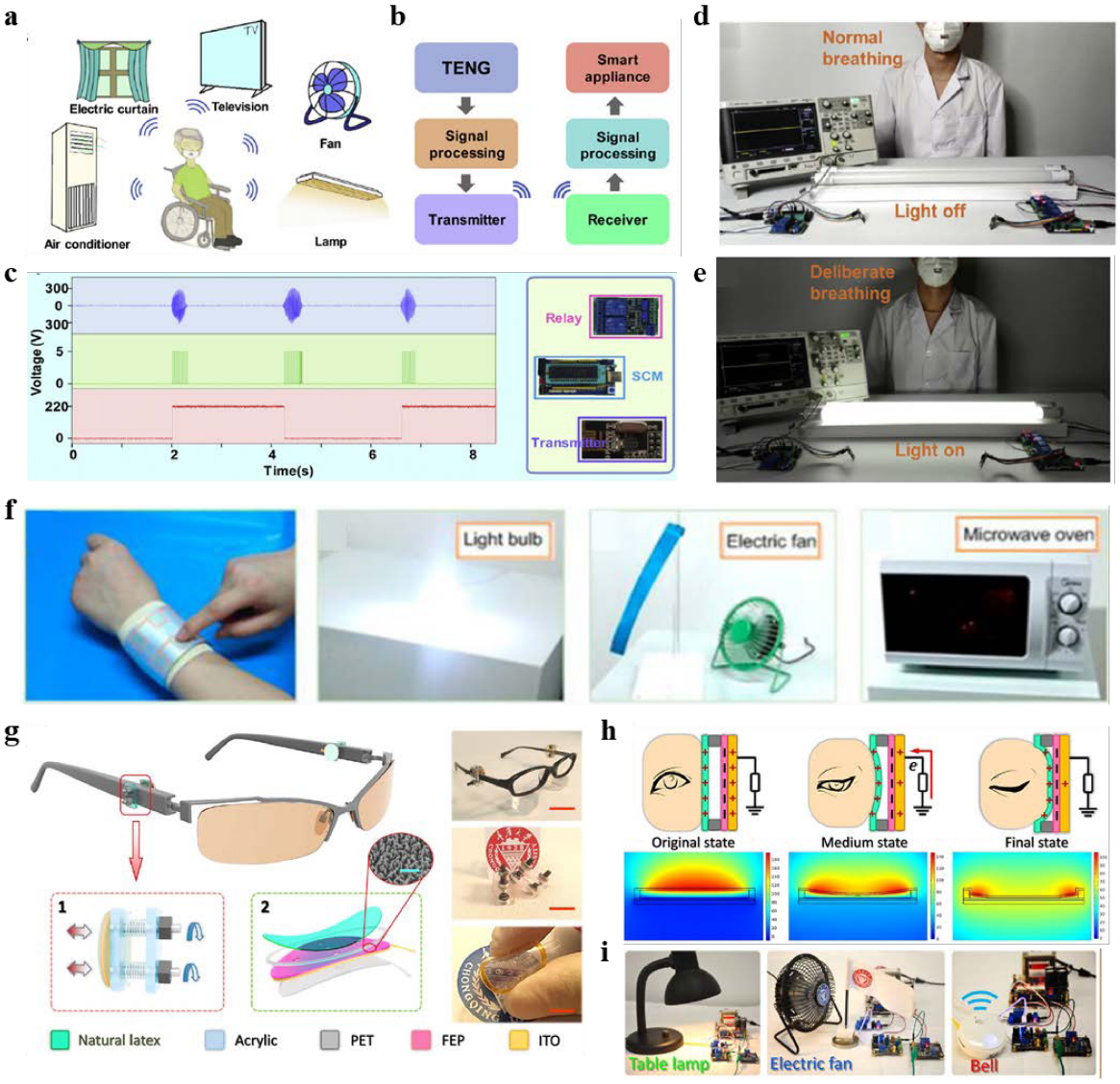

Figure 9. Control of household objects. a) Schematic illustrating household object control. b) Signal transmission and processing flow of the breathing operated HMI. c) Graph on the left shows the signals from the TENG (top), the switched square signal (middle), and electrical power (bottom). Right frame shows the electronics for signal processing and transmission including the relay, single-chip microcomputer (SCM), and transmitter. d) Normal breathing while the subject wore the TENG device on a mask did not turn on the light. e) Deliberate breathing turned on the light. f) Washable electronic textile (WET) mounted on the wrist (left) and control of home appliances (right frames). Reproduced with permission.[178] Copyright 2018, American Chemical Society. g) Eye-triggered mechanosensor on the frame of glasses.

Frame 1 shows the shows the structure of a fixation device. Frame 2 shows the schematic diagram for the msTENG. Right frames show the msTENG mounted on ordinary glasses (top), the fixation device (middle), and optical image of the msTENG (bottom). h) Mechanism of operation of the msTENG. Top frames show the behavior of the charges depending on the state of the eye. Bottom frames show the simulation results to illustrate the working principle. i) Various household objects including a lamp, fan, and doorbell controlled by the msTENG. a-e) Reproduced with permission.[176] Copyright 2019, Elsevier. g-i) Reproduced with permission.[173] Copyright 2017, American Association for the Advancement of Science.

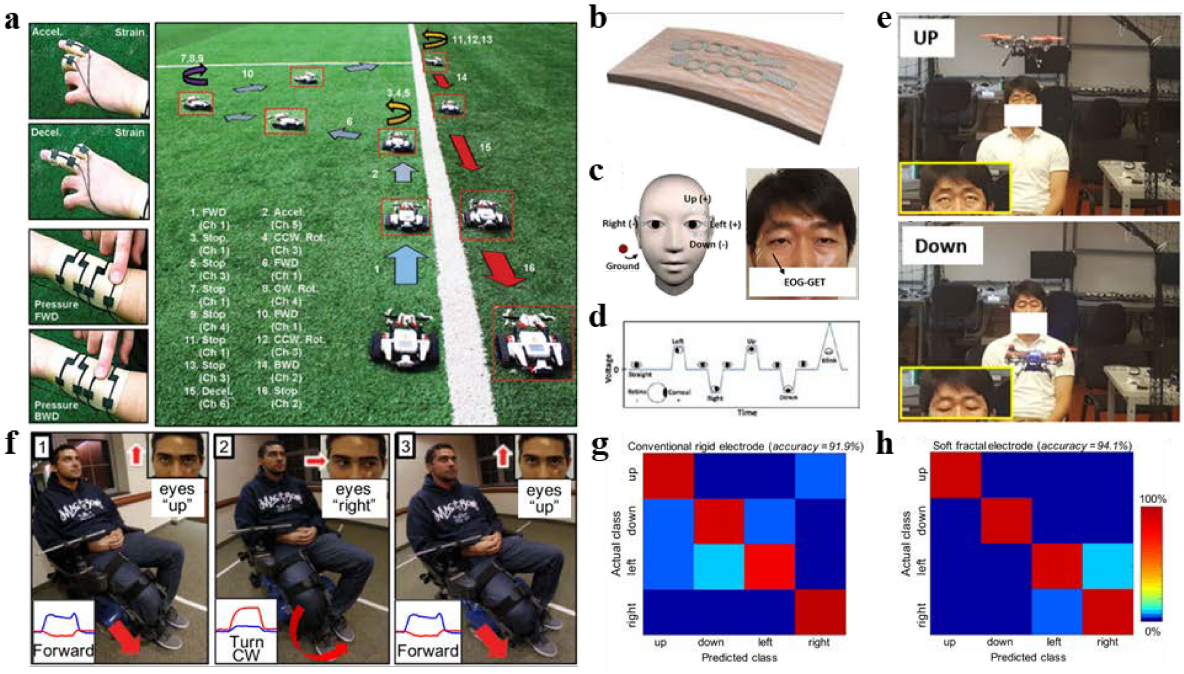

Figure 10. Control of mobile machines. a) PPSR based strain sensors and pressure sensors (left frames) used to control the movement of a mobile robot (right). Movement of different fingers allowed the robot to accelerate/decelerate while pressing the sensors on the forearm allowed for directional control. Reproduced with permission.[180] Copyright 2014, Wiley-VCH. b) Schematic of the EOG graphene electronic tattoo (EOG-GET) on skin. c) Arrangement of EOG-GET on the model (left) and on the human subject (right). d) Representative EOG signals for different eye movements. e) Quadcopter movement control by looking up to move the drone upwards (top) and looking down to move the drone downwards (bottom). f) Soft fractal structured electrodes used for EOG based control of a wheelchair. Insets show the voltage response of the electrodes for each eye movement. g) Confusion matrix for conventional electrodes. h) Confusion matrix for fractal electrodes showing the comparable accuracy for each class based on the detected EOG signals. b-e) Reproduced with permission.[183] Copyright 2018, Springer Nature. f-h) Reproduced with permission.[182] Copyright 2017, Elsevier.

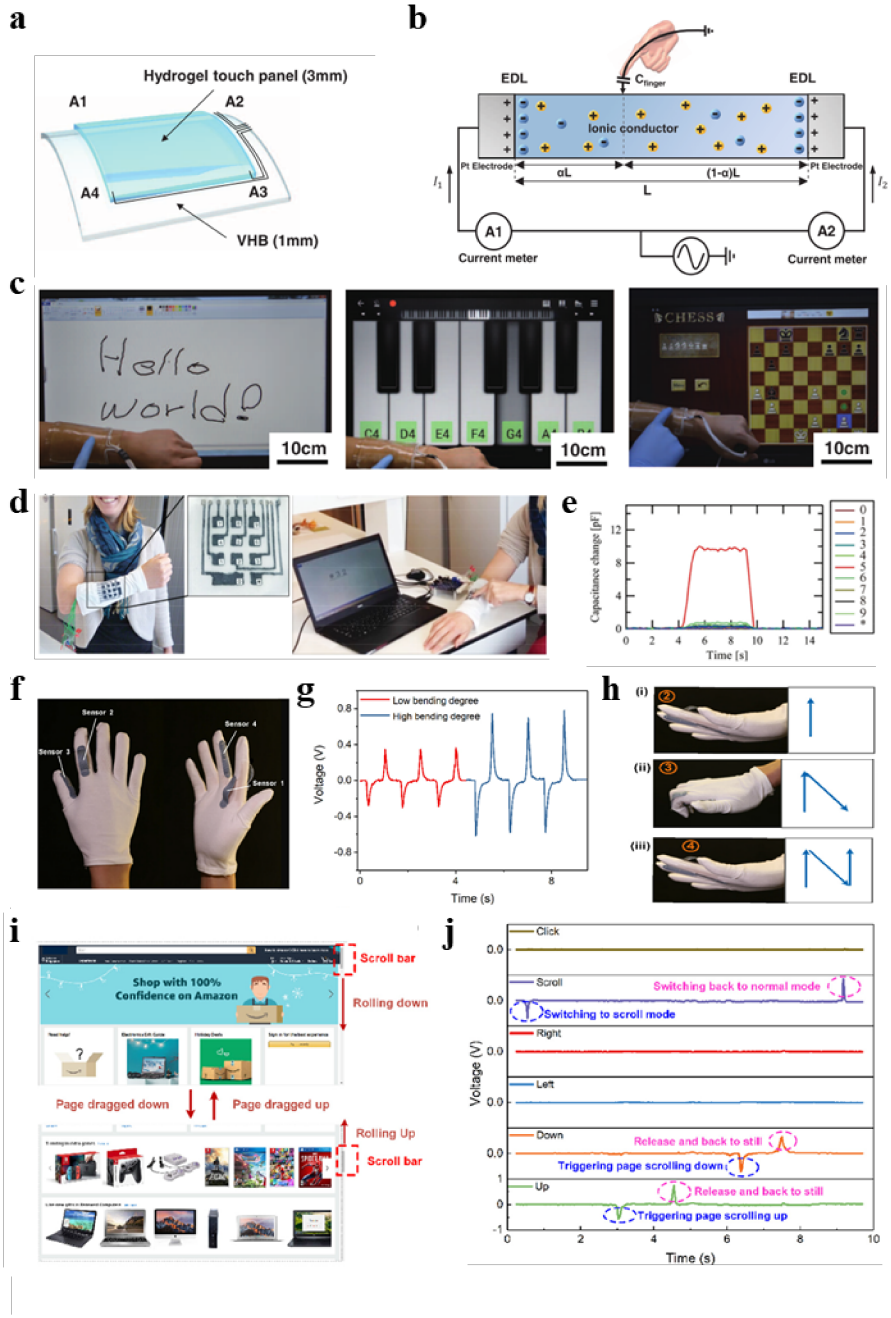

Figure 11. Tactile and motion sensors for virtual control. a) Mountable touch panel developed on a VHB substrate that served as insulation from the skin. b) Working mechanism of the stretchable, transparent ionic touch panel. When the finger contacts the panel, a closed circuit is created, resulting in a current flowing from both ends of the panel to the contact point. Reproduced with permission.[184] Copyright 2016, American Association for the Advancement of Science. c) The mounted touch panel controlling various computer applications for writing

words (left), playing music (middle), and playing a game (right). Reproduced with permission.[184] Copyright 2016, American Association for the Advancement of Science. d) Wearable keyboard based on PEDOT:PSS patterned onto a knitted textile and encapsulated by PDMS, mounted on the forearm of a subject (left). Setup for evaluating the input to the keyboard (right). e) Capacitance change when pressing the number 5 electrode. f) PEDOT:PSS based TENG on glove. g) Response of the TENG based on bending degree. h) Images of the hand motions to write the letter 'N' in a computer program. i) Scrolling up and down on an online shopping website. j) Real-time output from six TENGs to control the scrolling. a-c) Reproduced with permission.[184] Copyright 2016, American Association for the Advancement of Science. (d,e) Reproduced with permission.[185] Copyright 2016, Wiley-VCH. f-j) Reproduced with permission.[186] Copyright 2019, Elsevier.

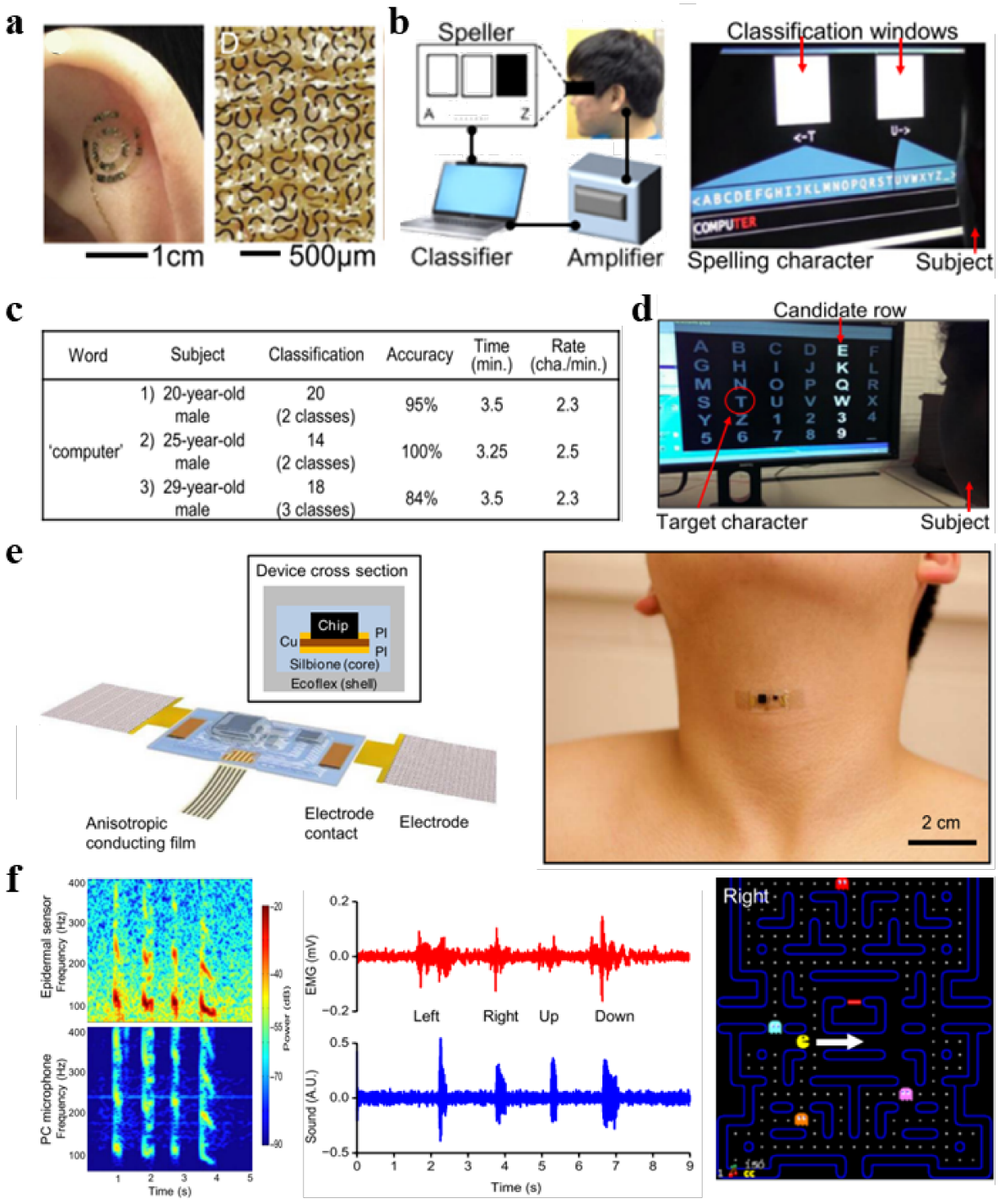

Word	Subject	Classification	Accuracy	Time (min.)	Rate (cha./min.)
'computer'	1) 20-year-old male	20 (2 classes)	95%	3.5	2.3
	2) 25-year-old male	14 (2 classes)	100%	3.25	2.5
	3) 29-year-old male	18 (3 classes)	84%	3.5	2.3

Figure 12. Physiological sensors for virtual control. a) Long-term epidermal (LTE) electrodes based on Au and PI designed in fractal layouts placed on the auricle (left) and magnified fractal layout (right). b) Schematic of experimental setup for controlling a brain-computer interface (left) and speller interface showing the visual stimulation, classification scheme, and subject performing the experiment. c) Performance of the subjects while trying to spell the word

'computer' using the LTE electrodes, average rate was 2.37 characters per minutes and average accuracy was 93%. The rate was about 2 times slower using the LTE electrodes as compared to that of a cap of 8-10 traditional electrodes. d) P300 based speller experiment used to detect event-related potentials which were used to identify the intended selections of the subject. e) Epidermal mechano-acoustic device schematic (left) and inset shows cross section. The device mounted on the vocal cords of a subject (right). f) Recorded speech with the mechano-acoustic and PC microphone showing comparable performance (left). EMG and vibrational signals measured simultaneously from the vocal cord (middle). Control of a video game using speech (right). a-d) Reproduced with permission.[187] Copyright 2015, United States National Academy of Sciences. e,f) Reproduced with permission.[188] Copyright 2016, American Association for the Advancement of Science.

Author biographies and photographs

Zhoulyu Rao is currently pursuing his Ph. D. degree in Material Science Engineering at the University of Houston, Houston, Texas, USA. He received his B.S. degree (2012) in Applied Chemistry from Xidian University, Xi'an, Shaanxi, China, and M.S. degree (2015) in Chemistry from University of Science and Technology of China, Hefei, Anhui, China. His current research interest is on development and microfabrication of soft devices for applications including 3D optoelectronics, biointerface, and wearable and implantable electronics.

Faheem Ershad is a PhD student at the University of Houston, Houston, TX, USA. He graduated with a Bachelor of Science in Biomedical Engineering (B.S.B.E.) in May 2018. He began working in Dr. Yu's group as an undergraduate student in 2017, and continued as a PhD student. He has investigated various soft electronics device technologies and their applications, ranging from implantable devices on the heart to portable, on-skin electrophysiological devices. His current research interest is in the development and applications of flexible/stretchable electronics for wearable/implantable health monitoring, disease treatment, and tissue engineering.

Cunjiang Yu received his Ph.D. degree in Mechanical Engineering from Arizona State University in 2010. He was a postdoctoral fellow in the Department of Materials Science and Engineering, University of Illinois at Urbana - Champaign during 2010 to 2013. He is currently the Bill D. Cook Associate Professor in the Department of Mechanical Engineering, University of Houston. His current research interests include wearable electronics, microelectromechanical systems, and biomedical implantable devices. He is a recipient of NSF CAREER Award, ONR Young Investigator Award, MIT Technology Review Top Innovator of China, etc.

Soft electronics is mechanically compliant and thus allows for intimate interfacing with human skin as health monitors and human-machine interfaces (HMIs), which clearly outperforms the conventional rigid and bulky electronics. This article reviews the recent development in soft skin-mountable electronics for health monitoring and HMIs and discusses the challenges and future directions.

Keywords: Soft electronics, stretchable electronics, skin, health monitoring, human-machine interfaces

Zhoulyu Rao, Faheem Ershad, Abdullah Almasri, Lei Gonzalez, and Cunjiang Yu*

Soft electronics for the skins: from health monitors to human-machine interfaces